

INITIAL STUDIES OF THE CHARMONIUM SYSTEM USING THE CRYSTAL BALL DATA AT SPEAR

Presented by E. D. Bloom<sup>\*</sup>  
(Representing the Crystal Ball Collaboration<sup>1]</sup>)  
Stanford Linear Accelerator Center  
Stanford University  
Stanford, CA 94305 U.S.A.

- 1] CalTech: R. Partridge, C. Peck, F. Porter. Harvard University: W. Kollmann, M. Richardson, K. Strauch. Princeton University: D. Aschman, T. Burnett, M. Cavalli-Sforza, D. Coyne, H. Sadrozinski. Stanford University (HEPL): R. Hofstadter, I. Kirkbride, H. Kolanoski, A. Liberman, J. O'Reilly, J. Tompkins. SLAC: E.D. Bloom, F. Bulos, R. Chestnut, J. Gaiser, G. Godfrey, C. Kiesling, M. Oreglia.

Abstract

First results from the Crystal Ball experiment (SP-24) are presented. In particular a preliminary analysis of 800K events at the  $J/\psi(3095)$  and 190K events at the  $\psi'(3684)$  gives new information on the existence of controversial states of the charmonium system. We find no signal for the X(2820).

Résumé

Nous présentons les premiers résultats de l'expérience Crystal Ball (SP-24) de SPEAR. En particulier une analyse préliminaire de 800K événements au  $J/\psi(3095)$  et de 190K événements au  $\psi'(3684)$  fournit des informations nouvelles sur l'existence d'états controversés du charmonium. Nous ne trouvons aucun signal correspondant au X(2820).

(Invited talk presented at the XIVth Rencontre de Moriond, Les Arcs-Savoie-France, March 11-23, 1979.)

---

\* Work supported by the Department of Energy, contract DE-AC03-76SF00515.

## I. Introduction

The need for a device which optimizes the detection of photons originating from electron-positron annihilations was foreseen<sup>2]</sup> even before the proliferation of  $\gamma$ -ray spectroscopies from the  $\psi$  and  $\psi'$  states, and culminated in the production of the "Crystal Ball" detector system. As shown in artist's rendition in Fig. 1, this system has as its principle component a thick segmented shell of 16 r.l. of NaI(Tl) surrounding cylindrical proportional and magnetostrictive wire chambers. Endcap detectors of 20 r.l. of NaI(Tl) behind magnetostrictive wire chambers supplement the main Ball, which covers 94% of  $4\pi$  ster., to  $\sim 98\%$  of  $4\pi$  ster. In addition (not shown in Fig. 1), muon detectors of interspersed iron and proportional tubes provide a sample (15% of  $4\pi$  ster.) of such final states around  $\theta_{CM} = 90^\circ$ .

The Crystal Ball was installed at SPEAR in the fall of 1978, and data taking began soon after. In this report I will present preliminary results from data obtained at the  $J/\psi(3095)$  and  $\psi'(3684)$  over the past 6 months.

## II. Apparatus

### a) NaI(Tl)

The thick NaI(Tl) shell has an outer radius of 66.0 cm and an inner cavity radius of 25.4 cm. It consists of 672 NaI(Tl) polycrin<sup>3]</sup> modules 40.64 cm (16 radiation lengths) in radial thickness, each of which is optically isolated from its neighbors and viewed by a separate phototube. The design of the Crystal Ball is based on the mathematics of an icosahedron, a 20-faced solid figure in which each face is an equilateral triangle of the same dimension. The projective geometry of R. Buckminster Fuller<sup>4]</sup> was used to divide the icosahedron (Fig. 2) into 4 minor triangles, and then each of these triangles into 9 triangles. The 720 resulting triangles are imbedded in the surface of a sphere containing the vertices of all the triangles. Finally, 24 triangles are omitted in two diametrically opposite regions in order to admit the electron-positron beams, which are made to collide at the center of the shell, and to allow cable access. In order to minimize the number of container walls (NaI(Tl) is hygroscopic and so must have a hermetic seal), to enhance the energy resolution and detector uniformity, the Crystal Ball is composed of just two hemispherical sections each containing 336 NaI(Tl) modules. The crystal modules within each hemisphere are separated by 0.4 mm of opaque paper and Al which should not absorb significant amounts of energy. The fundamental NaI(Tl) unit for measuring absorbed energy subtends  $\sim 0.14$  of  $4\pi$  ster. . Each unit has been internally compensated so that energy deposited at various points within it produces an output uniform to  $\pm 4\%$ .

### b) Electronics

In order to fully exploit the inherent precision of NaI(Tl) in  $\gamma$ -energy measurements, extreme care must be given to the selection of phototubes and the

design of the signal electronics. At SPEAR the dynamic range must extend from the noise at 0.05 MeV to at least 4000 MeV with  $\leq 1\%$  nonlinearity and costs had to be kept to a minimum. A fairly complete description of the system which has met these design goals is given in reference 5.

c) Chambers

The tracking chambers within the Ball are optimized to serve two separate functions: precise location of charged tracks and rapid multiplicity-related trigger information. The spark chambers and proportional chambers in the central detector are placed in the region between the beam pipe and the inner dome of the Ball. The inner and outermost chambers are 2 gap (4 plane) wire spark chambers with magnetostrictive readout. In between these two chambers are a double gap of proportional wire chambers with both anode readout and cathode strip readout. The innermost chamber subtends 94% of  $4\pi$  ster. while the outer chamber subtends 71% of  $4\pi$ . The MWPC system subtends 80% of  $4\pi$  ster.

The double gap of the proportional chambers, with 144 wires apiece, serves as the charged particle triggering element in our triggering scheme (cf. Section IV).

Each of 4 NaI(Tl) endcap assemblies of 15 modules each has 4 gaps of spark chambers, with magnetostrictive readout, in front of it. Thus the detector has charged particle tracking over its entire solid angle of 98% of  $4\pi$  ster.

d) Additional Systems

The detector has an associated luminosity monitor (see Fig. 1) which is expected to yield absolute luminosity measurements accurate to  $\pm 2\%$ . Also we have installed about  $\theta_{CM} = 90^\circ$  an outer hadron muon selector (OHMS) consisting of sandwiched proportional tubes and iron slabs. OHMS subtend 15% of  $4\pi$  ster. and will be used for muon identification and  $\pi/e$  separation.

### III. Calibration and Resolution

Absolute and intercalibration of the 732 modules of NaI(Tl) has proved to be the challenge in achieving the design resolution of the device. The presently used calibration procedure has been described elsewhere<sup>6]</sup>. In Fig. 3 is shown the resolution for electrons, obtained using a 54 modules prototype in an external test beam<sup>5]</sup>. The resolution obtained can be approximated well by,

$$\left. \frac{\Delta E}{E} \right)_{FWHM} = \frac{2.8\%}{4 \sqrt{E(\text{GeV})}} \quad (1)$$

Also shown in Fig. 3 are results obtained up to now by the full Crystal Ball at SPEAR. We find the present resolution to be about a factor of two higher than Eq. 1 would indicate. We believe that this discrepancy is caused by intercalibration errors among crystals and we have been developing a light pulser system to help solve the problem. As evidence for this hypothesis is presented a study

of Bhabha electrons in the detector at  $E = 1842 \text{ MeV}$  ( $E_{\text{CM}} = M_{\psi}$ ). Improvements in resolution can be seen in Fig. 4 to result from two sources. The curve shown by (+) results from our standard<sup>6]</sup> calibration procedure, and yields  $\Delta E/E)_{\text{FWHM}} = 9\%$ . Inclusion of the Bhabha electrons themselves in the intercalibration procedure yields the curve shown by (\*) and improves the resolution to  $\Delta E/E)_{\text{FWHM}} = 5.6\%$ . This step bears directly on the intercalibration problem. A final correction for nonuniformity across the face of each crystal yields the histogram and improves the resolution slightly to  $\Delta E/E)_{\text{FWHM}} = 4.7\%$ . The resolution expected from Fig. 3 and equation 1 is  $\Delta E/E)_{\text{FWHM}} = 2.4\%$ .

#### IV. Trigger Rate and General Event Characteristics

##### a) Typical Events

In Fig. 5 is shown a likely  $e^+e^- \rightarrow \mu^+\mu^-$  candidate. The mode of representation shows all the crystals in the Ball as small triangles; the endcap quadrants are shown without segmentation (each quadrant subtends  $\sim 1\%$  of  $4\pi$  ster.). Each major triangle (bold outline in Fig. 5) corresponds to a face of the underlying icosahedron (c.f. Fig. 2). These major triangles, or groups of 36, are numbered 1 thru 20. The hatched modules surrounding the endcap region are the so-called "Tunnel Modules." These modules have the poorest resolution and the highest rates of all the Ball modules proper, and so will be treated specially on occasion. This event was taken at  $E_{\text{CM}} = 4550 \text{ MeV}$ . Each crystal,  $i$ , with an energy deposition of  $E_i > 0.5 \text{ MeV}$  would show an integer 1-999 ( $> 999 = \text{xxx}$ ) representing the energy actually deposited in the crystal. This is also true for each endcap quadrant. What is clear from Fig. 5, and is typically true for all triggers, is the total lack of background (spurious energy deposition) in the Ball. Only two crystals show energy deposition in Fig. 5, Crystal 13 has 218 MeV and Crystal 420 has 200 MeV. These energies are expected for minimum ionizing particles passing radially thru the Ball ( $E_{\text{Min.ion}} \sim 200 \text{ MeV}$ ). The compact energy deposition profile left by muons is used to identify muon candidates for constrained events (cf. Section VII).

A very different type of event is shown in Fig. 6. This event is a Bhabha at  $E_{\text{CM}} = 7400 \text{ MeV}$ , the highest energy run at SPEAR this year. Again the Ball has very little spurious energy deposition, however, the high energy electrons have a large lateral spread and many crystals show energy deposition. This lateral shower spread characteristic is used for photons in determining the direction of the photon much more accurately than a single crystal size would allow. For example at  $E_{\gamma} = 1842 \text{ MeV}$  we presently achieve  $\sigma_{\text{Oprojected}} \lesssim 1^\circ$ , though a single crystal is  $\sim 12^\circ$  on a side. The angular resolution worsens as  $E_{\gamma}$  lowers; at  $E_{\gamma} \sim 100 \text{ MeV}$ ,  $\sigma_{\text{Oprojected}} \lesssim 2^\circ$  is presently obtained.

In Fig. 7 is shown a typical hadronic four charged prong (+3 neutrals) in the central chambers. The view shown is azimuthal i.e., a perpendicular section

thru the chambers and beam pipe. In the upper left of the figure is shown the energy deposition associated with each track as determined from our online software. Note: Figs. 5-7 were all obtained during data taking using online software.

b) Triggers and Rates

Our trigger strategy is one of multilevel triggers, each aimed at various elements of the possible physics. Table 1 summarizes the various triggers and their rates at representative energies. Also in Table 1 is a brief description of

Table 1  
Crystal Ball Event Triggers and Typical Rates

| Trigger Name               | Requirements   | Acceptance $\Delta\Omega/4\pi$        | $E_{CM}(\text{GeV})$ | $I_{\text{BEAM}}(\text{MA})$ | $\mathcal{L}(\mu\text{b}^{-1}\text{Sec}^{-1})$ | Trigger Rate(Hz) |
|----------------------------|--|---------------------------------------|----------------------|------------------------------|--|------------------|
| Total Energy               | Single discriminator on analog. sum of Ball Crystals excluding tunnel modules. Threshold $\sim 0.3 E_{CM}$   | 0.86<br>(Tunnel modules not included) | 3.095( $\psi$ )      | 4                            | 0.4  | 0.7              |
|                            |  |                                       | 3.684( $\psi'$ )     | 8                            | 1.1  | 0.9              |
|                            |  |                                       | 3.772( $\psi''$ )    | 11                           | 2.0  | 0.6              |
|                            |  |                                       | 7.40                 | 14                           | 4.0  | 0.3              |
|                            |  |                                       | 7.40                 | 35                           | 16.8   | 1.1              |
| Fast Trigger               | <ul style="list-style-type: none"> <li>• (<math>E_{\text{Top hemi}} &gt; \text{Min ionizing}</math>)</li> <li>• (<math>E_{\text{Bot hemi}} &gt; \text{Min ionizing}</math>)</li> <li>• (<math>E_{\text{TOTAL}} &gt; 600-800 \text{ MeV}</math>)</li> <li>• (<math>\pm 8\text{ns}</math> timing to Beam)</li> </ul> | 0.94<br>(Full Ball)                   | 3.095( $\psi$ )      | 4                            | 0.4  | 1.4              |
|                            |  |                                       | 3.684( $\psi'$ )     | 8                            | 1.1  | 1.1              |
|                            |  |                                       | 3.772( $\psi''$ )    | 11                           | 2.0  | 1.2              |
|                            |  |                                       | 7.40                 | 35                           | 16.8   | 2.2              |
| Multiplicity               | (Energy in $\geq 2$ major triangles) $\geq$ Min ionizing). (Hit in MWPC)   | 0.80<br>(defined by MWPC)             | 3.095( $\psi$ )      | 4                            | 0.4  | 1.6              |
|                            |  |                                       | 3.684( $\psi'$ )     | 8                            | 1.1  | 1.5              |
|                            |  |                                       | 3.772( $\psi''$ )    | 11                           | 2.0  | 1.4              |
|                            |  |                                       | 7.40                 | 35                           | 16.8   | 2.9              |
| Quark                      | (Two "groups of 9" <sup>a]</sup> back-to-back with $E_9 \geq 40 \text{ MeV}$ )<br>• ( $E_{\text{TOTAL}} > 140 \text{ MeV}$ )   | 0.94<br>(Full Ball)                   | 3.095( $\psi$ )      | 4                            | 0.4  | 1.1              |
|                            |  |                                       | 3.684( $\psi'$ )     | 8                            | 1.1  | --               |
|                            |  |                                       | 3.772( $\psi''$ )    | 11                           | 2.0  | 0.8              |
|                            |  |                                       | 7.40                 | 35                           | 16.8   | 1.8              |
| "Or" of all triggers above | Timing of Crystal Energy measuring strobe defined by beam cross in common  | 0.8<br>-0.94                          | 3.095( $\psi$ )      | 4                            | 0.4  | 2.2              |
|                            |  |                                       | 3.684( $\psi'$ )     | 8                            | 1.1  | 2.1              |
|                            |  |                                       | 3.772( $\psi''$ )    | 11                           | 2.0  | 2.2              |
|                            |  |                                       | 7.40                 | 35                           | 16.8   | 3.5              |

a] A major triangle, or group of 36, contains 4 groups of 9. The back-to-back requirement means one group of 9 is diametrically opposite to the other.

each trigger. These triggers listed are or'ed for the total trigger of the experiment. The total trigger rate is typically 2-3 Hz in the or. Given the generality and large overlap of the various triggers we expect very small systematic biases in the resulting event sample. Indeed, we expect essentially 100% efficiency for triggering on hadronic events.

c) QED as a check of the apparatus

In order to check the geometrical acceptance of the Ball, the luminosity monitor, and the inefficiency of the spark chamber system we have made a preliminary estimate of the cross section for the process

$$e^+e^- \rightarrow \gamma\gamma . \quad (2)$$

This preliminary result should not presently be used as an independent check of QED.

In Fig. 8 is shown the absolute differential cross section for the process of equation 2. The data is from  $324 \text{ nb}^{-1}$  at the  $\psi'$ ; note that no contribution from  $\psi' \rightarrow \gamma\gamma$  is expected. (We presently have on tape a total of  $\sim 1100 \text{ nb}^{-1}$  at the  $\psi'$ ). The Ball acceptance in this analysis has been conservatively limited to  $|\cos \theta| \leq 0.6$ . The data is shown with error bars, the theoretical QED result is the curve. Good agreement is obtained to the estimated systematic error of  $\pm 9\%$ .

Implicit in the design of the Ball is a flat azimuthal dependence over  $2\pi$  in  $\phi$ . To test for nonuniformity in  $\phi$ , QED events of the type of Eq. 2 were plotted versus  $\phi$ . In Fig. 9 the  $\phi$  distribution is shown where coplanarity of  $\pm 5^\circ$  is required between the two final state photons. The figure has a suppressed zero. Some azimuthal nonuniformity may be present at the  $\pm 5\%$  level; this uniformity is sufficient for our present analysis. Note that some nonuniformity is expected at  $\phi = 0^\circ, 180^\circ$ , the hemisphere boundaries.

d) Inclusive  $\pi^0$  and  $\eta$

In order to check the angular and energy resolution and calibration in an hadronically inclusive environment a search was made for inclusive  $\pi^0$ 's at the  $\psi'$  and inclusive  $\eta$  at the  $J/\psi$ . These energies were chosen since large signals were expected<sup>7]</sup>. In Fig. 10a is shown the  $\gamma\gamma$  mass distribution at the  $\psi'$ (3684) (in the mass range of the  $\pi^0$ ), and in Fig. 10b the  $\gamma\gamma$  mass distribution at the  $J/\psi$  (3095) (in the mass range of the  $\eta$ ). A total energy cut is made at the  $J/\psi$ (3095) of  $E_{\text{TOT}} > 2700 \text{ MeV}$ , also the  $\pi^0$  subtracted spectrum is shown in Fig. 10b.

Using the approximate relation,

$$\frac{\Delta m}{m} = \frac{1}{2} \sqrt{2 \left( \frac{\Delta E}{E} \right)^2 + \left( \frac{P_x}{m_x} \right)^2 \Delta \theta_{\gamma\gamma}^2} \text{ (rad)} , \quad (3)$$

One expects the  $\pi^0$  width to be dominated by angular resolution and  $\eta$  width to be dominated by energy resolution. Reasonable agreement with preliminary Monte Carlo calculations is obtained for both observed widths using previously mentioned angular and energy resolutions. Note that the known meson masses are closely reproduced.

#### V. Charmonium, Pre Crystal Ball

In Fig. 11<sup>8]</sup> is shown the state of experimental knowledge of the charmonium system as of 1977, the time of the Lepton-Photon Conference in Hamburg. At that time much of the charmonium picture made sense except for the glaring incongruity of the X(2820) and X(3455)<sup>9]</sup>. Since that time and still pre Crystal Ball two

experiments have added additional information on this subject; the DESY-Heidelberg<sup>10]</sup> Doris results and Mark II<sup>11]</sup> results at SPEAR. These results as well as previous results obtained from reviews<sup>8,12]</sup> are shown in Table 2. The problem of the X(3455) looks like it has gone away, that of the X(2820) remains; however, a new one, X(3591), has emerged.

Table 2  
Representative J/ψ, ψ' Cascade Results Pre Crystal Ball<sup>8,10,11,12]</sup>

| State | Status | (a)          | (b)                        | Experiments  |
|-------|--------|--------------|----------------------------|--|
|       |        | Br(ψ') → γX) | Br(ψ → γX)<br>• Br(X → γψ) |  |
| 3.415 | Yes    | 0.07 ± 0.02  | < 0.0025                   | (a) M P <sup>2</sup> S <sup>3</sup> D, Mark I<br>(b) DESY-Heidelberg                 |
| 3.455 | ?      | < 0.025      | < 0.0012                   | (a) M P <sup>2</sup> S <sup>3</sup> D, (b) Mark II                                   |
| 3.503 | Yes    | 0.07 ± 0.02  | 0.023 ± 0.004              | (a) M P <sup>2</sup> S <sup>3</sup> D, (b) DASP,<br>Mark I<br>Pluto, DESY-Heidelberg |
| 3.551 | Yes    | 0.07 ± 0.02  | 0.013 ± 0.003              | (a) M P <sup>2</sup> S <sup>3</sup> D, (b) Mark I<br>DASP, Pluto, DESY-Heidelberg    |
| 3.59  | ?      | --           | 0.0018 ± 0.0006            | (b) DESY-Heidelberg  |

No other states are observed for ψ'.

Note: upper limits are 90% C.L.

Only one cascade observed for the J/ψ.

$$\begin{array}{l} \psi \rightarrow \gamma X(2820) \\ | \\ \rightarrow \gamma\gamma \end{array}$$

$$\text{Br } \begin{array}{l} \psi \rightarrow \gamma X \\ | \\ \rightarrow \gamma\gamma \end{array} = 1.4 \pm 0.4 \cdot 10^{-4}$$

For inclusive production of the X(2820):

$$\text{Br } (\psi \rightarrow \gamma X(2820)) < 0.017, \text{ M P}^2 \text{ S}^3 \text{ D.}$$

The preliminary Crystal Ball results presented here have much to add on the above issues.

Shown in Fig. 12 are recently published results from the M P<sup>2</sup> S<sup>3</sup> D Collaboration<sup>13]</sup>. Figure 12a shows their inclusive γ spectrum obtained from ~ 100 nb<sup>-1</sup> at the ψ, Fig. 12b shows the inclusive γ spectrum obtained from ~ 600 nb<sup>-1</sup> at the ψ', Fig. 12c shows the spectrum of Fig. 12b minus an empirical background shown as the dotted line in Fig. 12b. In Fig. 13 is shown a Crystal Ball inclusive spectrum, a preliminary analysis of 324 nb<sup>-1</sup> at the ψ' (~ 180K ψ' events). The contribution of tunnel modules and equatorial modules is treated

specially in this inclusive spectrum. Note the suppressed zero. This analysis uses  $< 1/4$  of our data on tape and does not use our latest intercalibration procedures.

VI. Inclusive  $\gamma$  Production from  $\psi'$  (3684)

$$(\psi' \rightarrow \gamma \chi)$$

Figure 14a displays the preliminary inclusive  $\gamma$  spectrum from  $\psi'$ , shown with an empirical background fit to the spectrum (solid line). An attempt has been made to remove  $\pi^0$  contamination from the inclusive spectrum, but up to now our procedures have only been partially successful.  $0.64 \pi^0$ 's per event are removed on average in the spectrum of Fig. 14a. In Fig. 14b is shown the  $\gamma$  spectrum obtained after the subtraction of the empirical background fit. Using a relative normalization procedure one can obtain relative rates of the major transitions. At the present time full Monte Carlo simulation are not available which would allow the calculation of the efficiency for our inclusive  $\gamma$  yield. To obtain an absolute normalization we normalize our extracted yield of  $\chi(3503)$ , the  $1^{++}$  state, to the results of M P<sup>2</sup> S<sup>3</sup> D<sup>13]</sup> shown in Table 2. Our relatively normalized results along with measurements of the  $\gamma$  energies are shown in Table 3:

Table 3  
Preliminary Crystal Ball  $\psi'$  inclusive  $\gamma$   
 $\chi(3503)$  Yield Normalized to M P<sup>2</sup> S<sup>3</sup> D<sup>13]</sup> Result

| State        | J <sup>PC</sup> | Previous<br>E <sub><math>\gamma</math></sub> <sup>a]</sup><br>(MeV) | Crystall<br>Ball, E <sub><math>\gamma</math></sub> <sup>b]</sup><br>(MeV) | Br( $\psi' \rightarrow \gamma \chi$ ) |
|--------------|-----------------|---|---|---------------------------------------|
| $\chi(3551)$ | $2^{++}$        | $131 \pm 4$   | $127 \pm 2$   | $0.06 \pm 0.01$                       |
| $\chi(3503)$ | $1^{++}$        | $177 \pm 4$   | $174 \pm 3$   | 0.071 (Normalized)                    |
| $\chi(3414)$ | $0^{++}$        | $260 \pm 3$   | $264 \pm 4$   | $0.07 \pm 0.01$                       |
| $\chi(3455)$ | ?               | 222   | $222 \pm 15$  | $< 0.006$ (90% C.L.)                  |

a] We take the best previous measure of the  $\chi$  energies to be from reference 14. E <sub>$\gamma$</sub>  for X(3455) was calculated.

b] An estimated 2% systematic error is not included.

We find agreement in the ratios with previous experiments<sup>13,15]</sup> for the well-established  $\chi$  states. Our upper limit on inclusive X(3455) production is considerably stronger than previous results.

VII. Cascade Radiative Decays of  $\psi'$  (3684)

$$\begin{array}{l}
 (\psi' \rightarrow \chi \gamma) \\
 \quad \quad \quad \downarrow \\
 \quad \quad \quad \rightarrow \gamma \psi \\
 \quad \quad \quad \quad \quad \quad \downarrow \\
 \quad \quad \quad \quad \quad \quad \rightarrow e^+ e^-)
 \end{array}$$

In Fig. 15a is shown the state of knowledge of the cascade radiative decays

in late summer of 1977. The data from three experiments are shown in the plot, DASP, PLUTO and SLAC-LBL. At the time of this conference (Moriond) only the SLAC-LBL results<sup>14]</sup> have been published. On examining the figure, one notes that all states shown have been seen by all experiments listed. Indeed the  $\chi(3455)$  appears on as strong a basis (or stronger) than the  $\chi(3551)$ . Also, the signal from the  $\chi(3414)$  seems clear. The theorists were perplexed with these results, but the number of confirming experiments was hard to argue against.

Enter DESY-Heidelberg<sup>10]</sup>, Mark II<sup>11]</sup>, and the Crystal Ball and a very different picture emerges. Indeed, we are not likely to see a final answer until all Crystal Ball data is analyzed sometime late this summer. In Fig. 15b is shown the DESY-Heidelberg results. The  $\chi(3455)$  and  $\chi(3415)$  have almost disappeared, and a new state X(3591) is claimed. The DESY-Heidelberg results are also shown in Table 2. (The recent Mark II results<sup>11]</sup> are shown in the table for X(3455).)

In Fig. 16 is shown a Monte Carlo simulation of what one would expect to observe with the Crystal Ball using presently known estimates of branching ratios for the well-established  $\chi$  states, and 180K  $\psi'$  decays. The data are presented on a  $\log E_{Hi}^Y$  vs.  $\log E_{Low}^Y$  scale to allow optimum observation of the expected Doppler broadening of the second  $\gamma$  emitted in the cascade. With our presently obtained resolution, the Doppler broadening is barely visible, though 2-D fits of our resolution functions indicate a significant Doppler broadening in the real data (and Monte Carlo). The preliminary result of our data analysis of 180K  $\psi'$  decays is shown in Fig. 17. The observed numbers of events (indicated on the figures) is in excellent agreement with previously observed branching ratios for the well-established  $\chi$  states. In Table 4 preliminary quantitative estimates of branching

Table 4

Preliminary Crystal Ball Branching Ratios for the Cascade Decays of  $\psi'(3684)$

| State        | $J^{PC}$ | Crystal Ball<br>$E_{Low}^Y$ a)<br>(MeV) | $Br(\psi' \rightarrow \gamma\chi) \cdot Br(\chi \rightarrow \gamma\psi)$ |
|--------------|----------|---|--|
| $\chi(3551)$ | $2^{++}$ | $128 \pm 2$                             | $0.013 \pm 0.003$  |
| $\chi(3503)$ | $1^{++}$ | $173 \pm 3$                             | $0.025 \pm 0.006$  |
| $\chi(3414)$ | $0^{++}$ | --                                      | $0.0009 \pm 0.0005$ (Poor Signal)  |

a] Possible systematic error of  $\pm 2\%$  not included.

ratios are made. The simplicity of this final state has allowed Monte Carlo calculations of acceptance to be completed. The Monte Carlo calculation assumes the usually assumed  $J^P$  assignment to the  $\chi$  states (see Table 4). Note that both electron and muon decays of the  $J/\psi(3095)$  are included. As mentioned in Section IV(a), the  $\mu$ 's are identified by their compact pattern of energy deposition in the Ball. Also, no kinematic fitting has been performed on the events as yet. The

$\gamma\gamma e^+e^-$  events are 5-C, while the  $\gamma\gamma \mu^+\mu^-$  are 3-C.

One expects that improvements in energy resolution, kinematic fitting and four times the data will make a significant impact on our results. Thus my remarks at this conference are guarded. That the  $\chi(3455)$  is much reduced from the earlier Mark I result<sup>14]</sup> is clear; however, that a state may or may not exist in the 3470 region is not so clear from our present results. Also, the case for or against the  $X(3591)$  must await more data. We see 3 or 4 events in this region in Fig. 17 while we would expect about 16 events using the DESY-Heidelberg branching ratios. Thus Table 4 contains numbers only for the well-established states.

VIII. Inclusive  $\gamma$  Production from  $J/\psi(3095)$   
 $(\psi' \rightarrow J/\psi + \gamma)$

In Fig. 18 is presented a preliminary inclusive  $\gamma$  spectrum obtained from 87K  $J/\psi(3095)$  decays. We presently have on tape 900K  $J/\psi$  events. The qualitative difference of this spectrum as compared to that in Fig. 13 is clear.

There is no obvious structure from 50 MeV to 1 GeV. A preliminary analysis of 300K  $J/\psi$  decays (no figure) has yielded the result<sup>16]</sup>,

$$\begin{aligned} \text{Br}(J/\psi \rightarrow \gamma X) &< 0.5\% \text{ (90 C.L.)} \\ 100 \text{ MeV} &< E_\gamma < 1000 \text{ MeV.} \end{aligned} \quad (4)$$

The limit is a factor of 3 stronger than previous limits<sup>13]</sup>. If one uses the DASP<sup>12]</sup> result for

$$\begin{aligned} \text{Br}(J/\psi \rightarrow \gamma X(2820)) &= 1.4 \pm 0.4 \times 10^{-4} \\ &\quad \downarrow \\ &\quad \gamma\gamma \end{aligned} \quad (5)$$

our limit implies

$$\text{Br}(X(2820) \rightarrow \gamma\gamma) > 2.8\% \quad (6)$$

This result is a factor of 20 higher than expected in simple charmonium models<sup>17]</sup>.

IX.  $J/\psi(3095) \rightarrow \gamma\gamma\gamma$

We have performed a preliminary analysis of our full data sample of (910K  $\pm$  91K)  $J/\psi'$  ( $325 \text{ nb}^{-1}$ ), looking for events of the type

$$J/\psi(3095) \rightarrow \gamma\gamma\gamma. \quad (7)$$

A total of 3943  $\gamma$  events passed our cuts; a typical such event is shown in Fig. 19. As can be seen from the figure, these events are very clean and easily recognized. The cuts included requirements of no charged tracks, only three particles with essentially the full CM energy of the  $J/\psi$  measured, and for all three photons,  $|\cos \theta_{\gamma\gamma}| < 0.90$  to avoid overlap problems. The geometrical acceptances were obtained by Monte Carlo. Each event was kinematically fit (3C fit). The resulting Dalitz plot is shown in Fig. 20.

The events in the Dalitz plot come from various processes: a)  $\psi \rightarrow \eta\gamma$ , b)  $\psi \rightarrow \eta'\gamma$ , c)  $\psi \rightarrow \gamma\gamma\gamma$  (Direct decay), d)  $e^+e^- \rightarrow \gamma\gamma\gamma$  (QED), and perhaps, e)  $\psi \rightarrow X(2820)\gamma$ .

In Fig. 21 is shown the low mass projection of the Dalitz plot of Fig. 20.

The data are displayed vs.  $M$  rather than  $M^2$  for ease of comparison. A clear  $\eta$  and  $\eta'$  signal is seen. The calculated QED yield (d) above) is shown as a dotted line. After correction for QED, and acceptance we obtain<sup>16]</sup>

$$\text{Br}(J/\psi \rightarrow \gamma\eta) = (1.02 \pm 0.17) \times 10^{-3}, \quad (8)$$

$$\text{Br}(J/\psi \rightarrow \gamma\eta') = (5.9 \pm 1.5) \times 10^{-3} \quad (9)$$

$$\text{Br}(J/\psi \rightarrow \gamma\eta') / \text{Br}(J/\psi \rightarrow \gamma\eta) = 5.8 \pm 1.4 \quad (10)$$

The  $\eta\gamma$  branching fraction and resulting ratio of  $\eta\gamma'$  to  $\eta\gamma$  are higher than the other experiments by about a factor of two. These results as well as those following for the X(2820) have been obtained by direct use of the projections of the Dalitz plot, and by a two-dimensional fit of processes a)  $\rightarrow$  e) above to the Dalitz plot. Both techniques yield the same results to within 10%.

In Fig. 22 the high mass projection of the Dalitz plot is shown. Calculated absolute values for  $\gamma\eta$  and  $\gamma\eta'$  (processes (a) and (b) above) are shown. The QED,  $\eta$  and  $\eta'$  calculations used a Monte Carlo and so the results fluctuate. In this preliminary analysis no X(2820) signal is observed. Given the DASP result (cf. Table 2), and an X(2820) narrower than our mass resolution of  $\lesssim 25$  MeV, FWHM in this mass region, we would expect to observe 53 events in 2 bins centered on 2820. We observe 6 events above background yielding<sup>16]</sup>

$$\text{Br}(J/\psi \rightarrow \gamma X(2820)) < 0.3 \times 10^{-4} \text{ (90\% C.L.U.L.)}, \quad (13)$$

|  
→  $\gamma\gamma$  .

### X. Conclusions

Though these results are preliminary, their general trend is to give new hope for the simpler charmonium models. The apparent absence of X(2820), the much smaller branching ratio for X(3455) than previously reported are supportive of naive charmonium. However, the pseudo-scalars are a necessary element of the model; their existence must be established if the theory is to be believed.

The search for these states is a major part of the Crystal Ball program and we expect some answers soon.

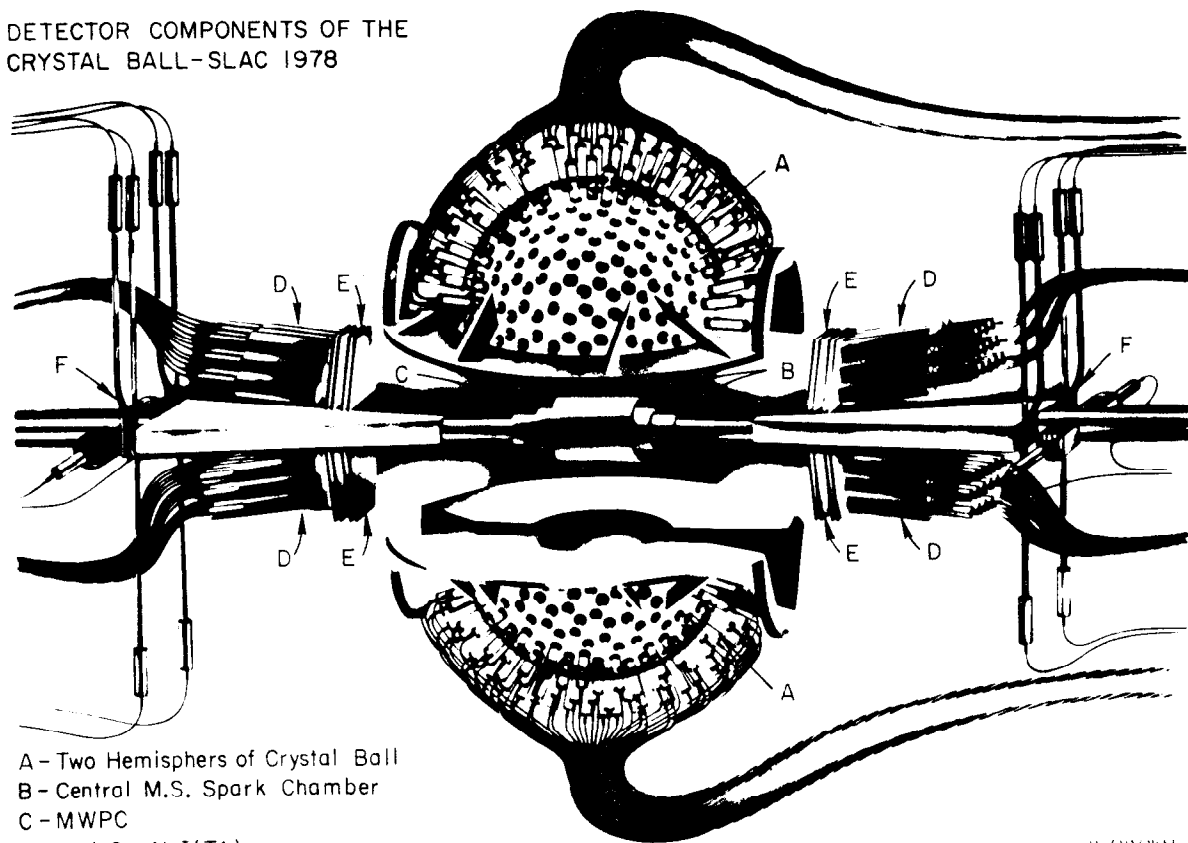
### References

- 1) Present Crystal Ball Collaboration: CalTech: R. Partridge, C. Peck, F. Porter. Harvard University: W. Kollmann, M. Richardson, K. Strauch. Princeton University: D. Aschman, T. Burnett, M. Cavalli-Sforza, D. Coyne, H. Sadrozinski. Stanford University (HEPL): R. Hofstadter, I. Kirkbride, H. Kolanoski, A. Liberman, J. O'Reilly, J. Tompkins. SLAC: E. Bloom, F. Bulos, R. Chestnut, J. Gaiser, G. Godfrey, C. Kiesling, M. Oreglia.
- 2) E. D. Bloom, et al., (1974), "Report on Neutral Particle Detectors and QED," 1974 PEP Summer Study, PEP-137, PP 218-278.
- 3) Polyscin is a registered Trade Mark of the Harshaw Chemical Co. of Solon, Ohio. The NaI(Tl) portions of the detector were built in collaboration

with Harshaw.

- 4) J. D. Clinton, R. B. Fuller (1970), "Advanced Structural Design Concepts for Future Space Missions," NASA Contract NGR 14-008-002.
- 5) Y. Chan, et al., (1978), "Design and Performance of a Modularized NaI(Tl) Detector," IEEE Transactions on Nuclear Science, V. NS-25, Number 1, PP 333-339.
- 6) I. Kirkbride, et al., (1979), "Use of a Low Energy Photon Accelerator for Calibrating a Large NaI(Tl) Array in a High Energy Physics Experiment," IEEE Transactions on Nuclear Science, V. NS-26, Number 1, PP 1535-1538.
- 7) G. J. Feldman in "Proceedings of the 5th International Conference on Experimental Mesons Spectroscopy," (1977) (Northeastern University Press, Boston 1977) edited by E. Von Goeler and R. Weinstein, P. 1.
- 8) G. Flügge (1978), "Particle Spectroscopy," DESY 78/55. (Invited talk at the 19th International Conference on High Energy Physics, Tokyo, Japan, August 1978).
- 9) K. Gottfried, (1977), "The Spectroscopy of the New Particles," Proceedings 1977 International Symposium on Lepton and Photon Interactions at High Energies. DESY, Editor F. Gutbrod.
- 10) W. Bartel, et al., (1978), "Cascade Radiative Decays of  $\psi'$ (3684) and Evidence for a New Intermediate State of Even C-Parity," Phys. Lett. 79B, P 492.
- 11) Report of D. Scharre, this Conference.
- 12) B. H. Wiik and G. Wolf (1978), "A Review of  $e^+e^-$  Interactions," DESY 78/23.
- 13) C. J. Biddick, et al., (1977), "Inclusive Gamma Ray Spectra from  $\psi$ (3095) and  $\psi'$ (3684) Decays," Phys. Rev. Lett. 38, P 1324.
- 14) W. M. Tanenbaum, et al., (1978), "Radiative Decays of the  $\psi$ (3684) into High Mass States," Phys. Rev. D17, PP 1731.
- 15) J. S. Whitacker, et al., (1976), "Radiative Decays of  $\psi$ (3095) and  $\psi$ (3684)," Phys. Rev. Lett. 37, PP 1596.
- 16) These results are updated from those I presented at the Conference in March. They correspond to those presented by F. Bulos at the APS Washinton Meeting in April 1979.
- 17) Report of A. Billoire, this Conference.

DETECTOR COMPONENTS OF THE  
CRYSTAL BALL-SLAC 1978



- A - Two Hemispheres of Crystal Ball
- B - Central M.S. Spark Chamber
- C - MWPC
- D - End Cap NaI(Tl)
- E - End Cap M.S. Spark Chambers
- F - Luminosity Monitor

5-79

W. ZAWOJSKI

3026A1

Fig. 1

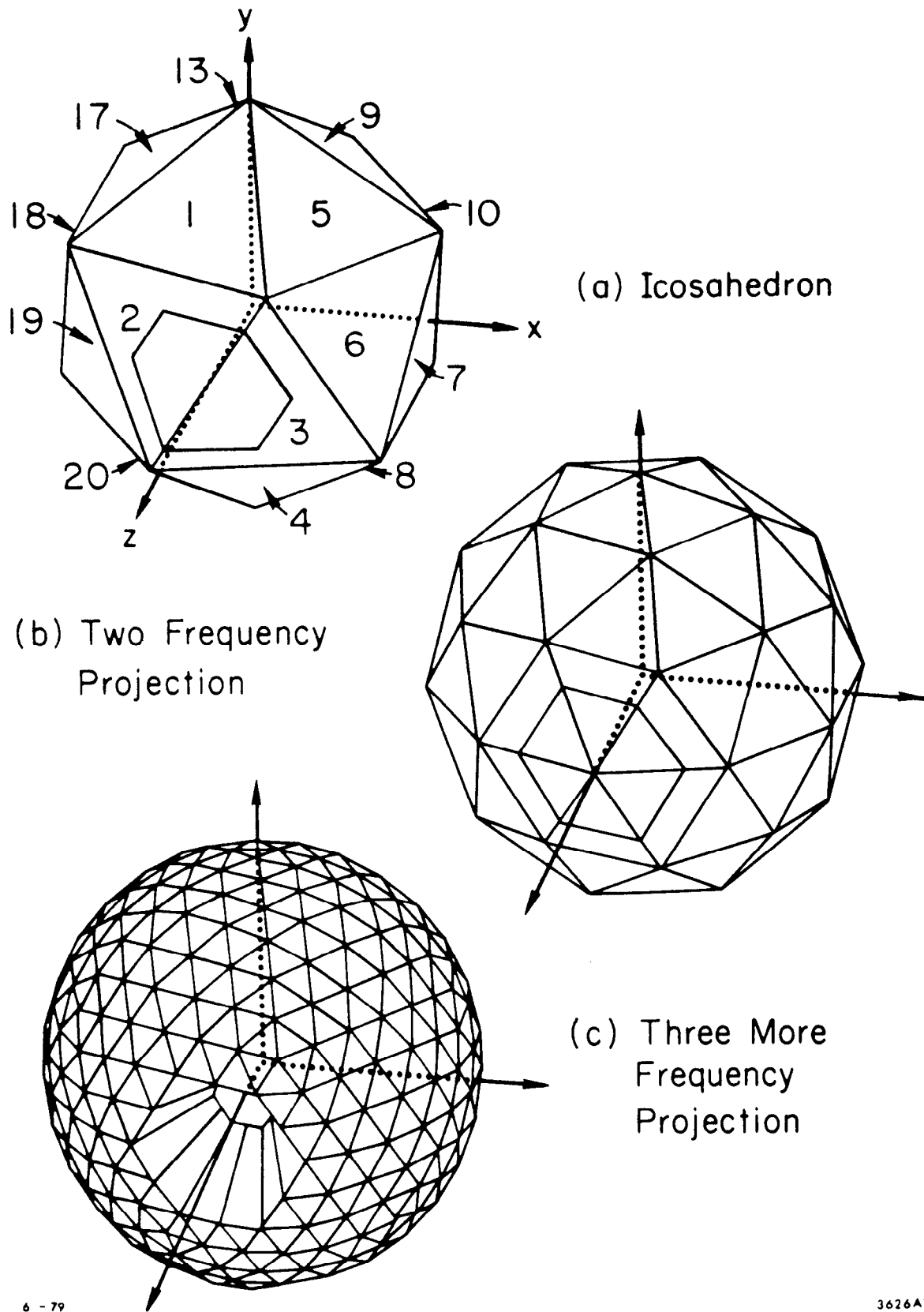
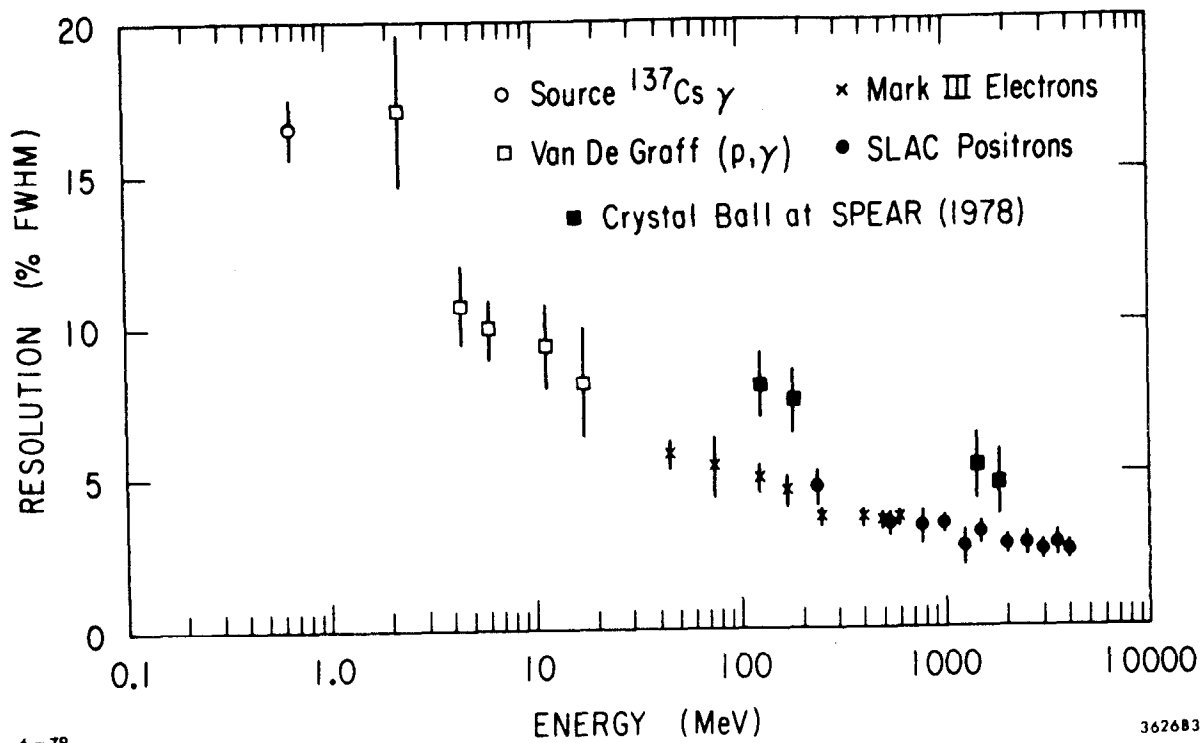


Fig. 2  
Geometry of the Crystal Ball



6-79

362683

Fig. 3

Prototype resolution curve with  
actual Crystal Ball data over  
plotted

SUM 13 - ALL EVENTS

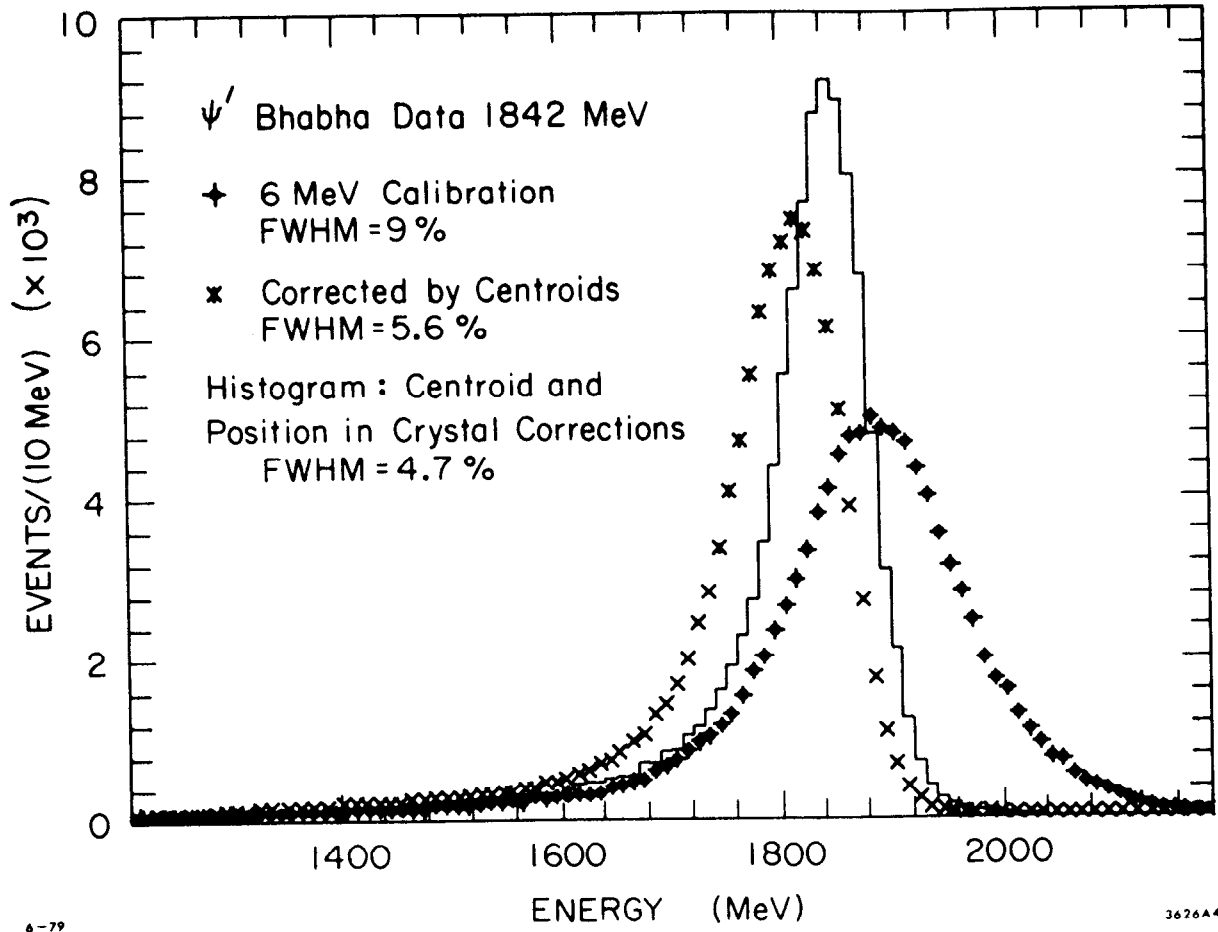


Fig. 4

Bhabha resolution at  $E_{CM} = M_{\psi'}$

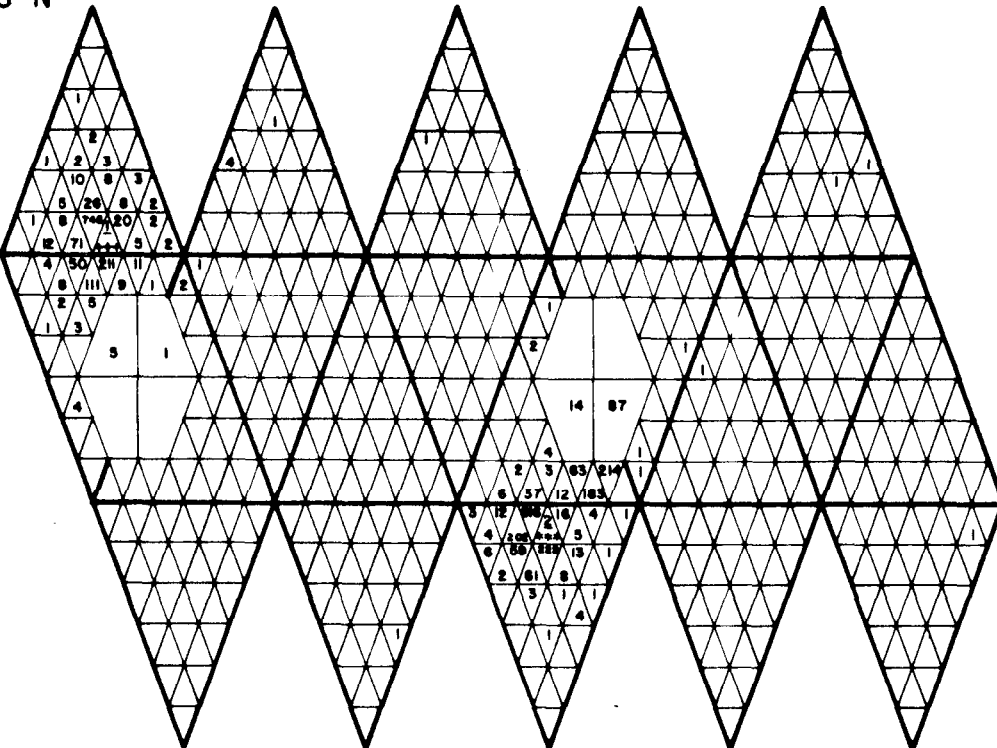


RUN #1350 EVENT #125 ETOT=7577 (MeV) ECM = 7400 (MeV)

\* CR TRK T  
1 3700 3796 N  
2 3690 3748 N

$e^+e^-$   
EVENT

$E_i > 0.5$  MeV  
WILL SHOW  
UP IN THIS  
PICTURE



\*\*\*1691 IN 415

...

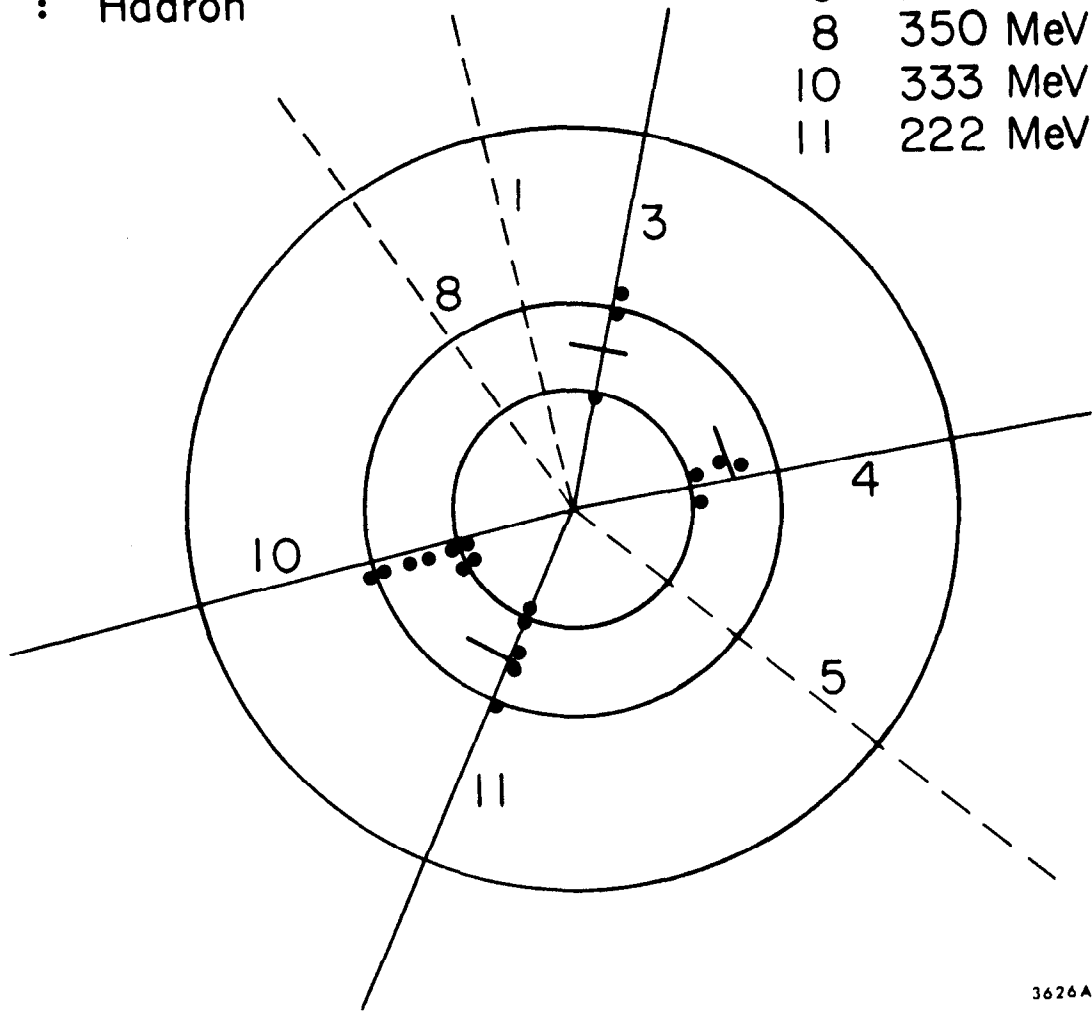
\*\*\*2445 IN 32

Fig. 6  
 $e^+e^- \rightarrow e^+e^-$  Event at 7.4 GeV

EVENT = 4680 = 2.1850 GeV  
RUN = 2137

Trigg : 162000  
Latch : 400  
Asym : 0.155  
Type : Hadron

|    |         |
|----|---------|
| 1  | 46 MeV  |
| 3  | 231 MeV |
| 4  | 666 MeV |
| 5  | 282 MeV |
| 8  | 350 MeV |
| 10 | 333 MeV |
| 11 | 222 MeV |



6-79

3626A7

Fig. 7  
Hadronic 4-charged prong in the  
central chambers

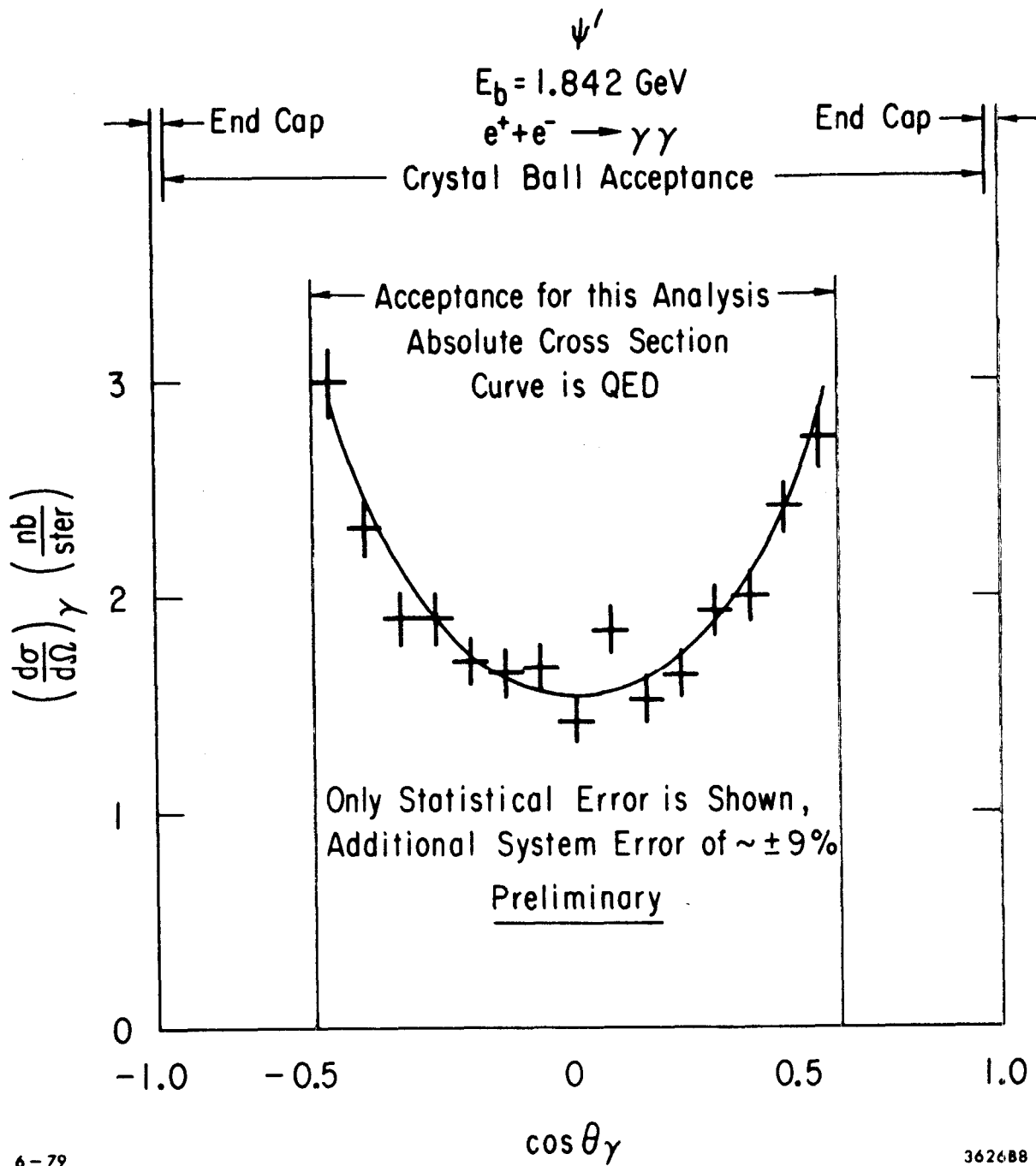
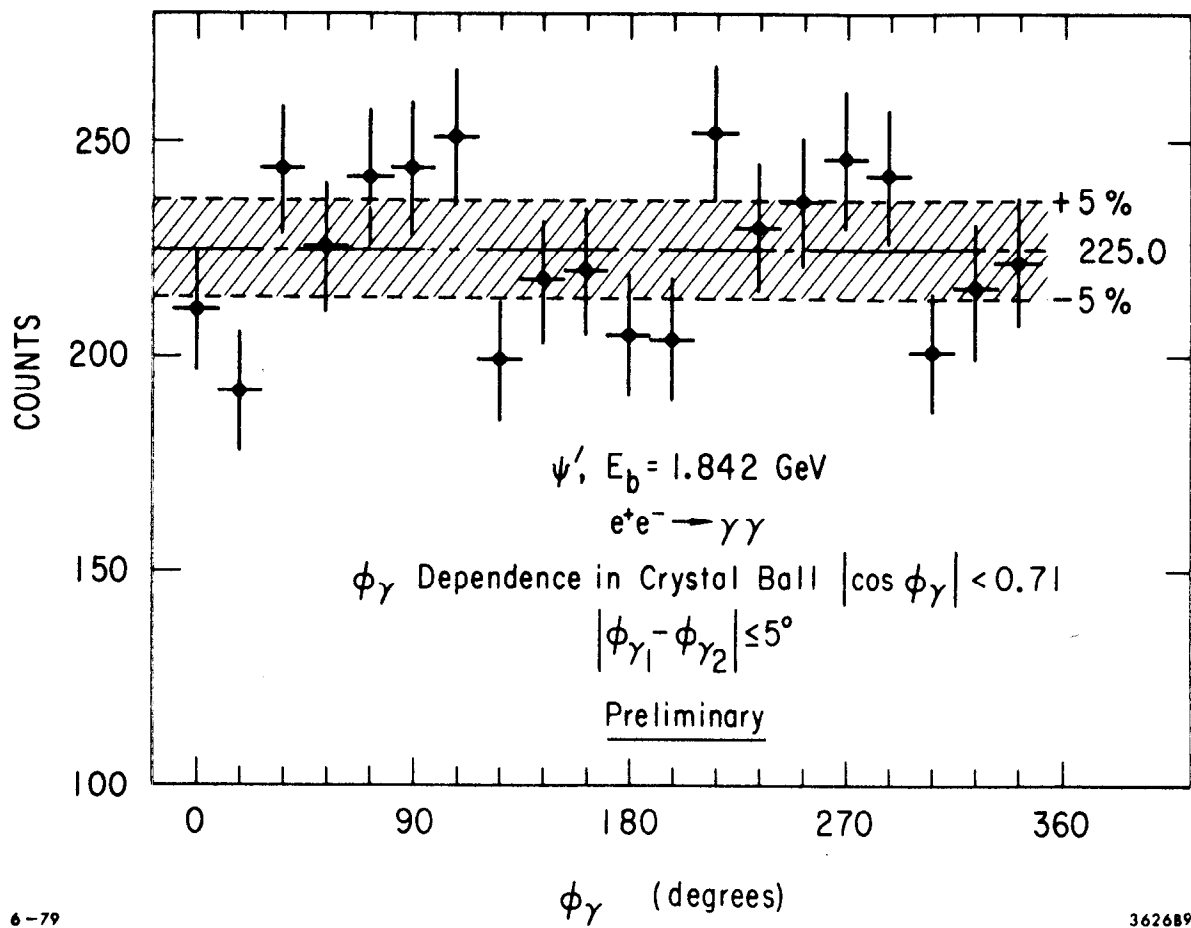


Fig. 8  
 Absolute cross section for  $e^+e^- \rightarrow \gamma\gamma$  at  $E_{\text{CM}} = M_{\psi'}$



6-79

362689

Fig. 9  
 $\phi$  Distribution for  $\gamma$ 's from  $e^+e^-$   
 $\rightarrow \gamma\gamma$

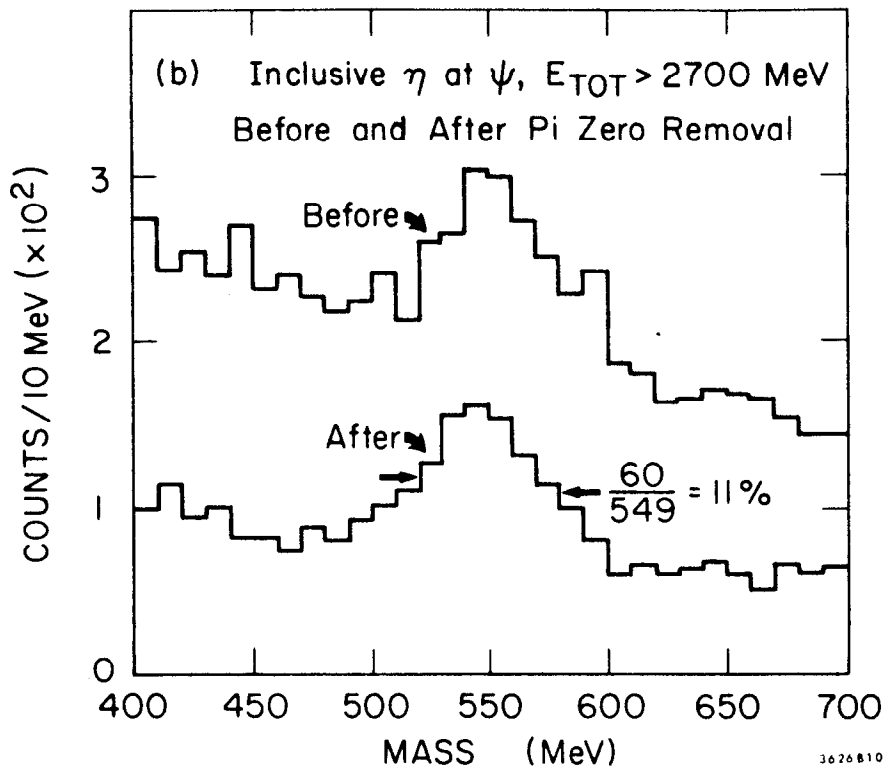
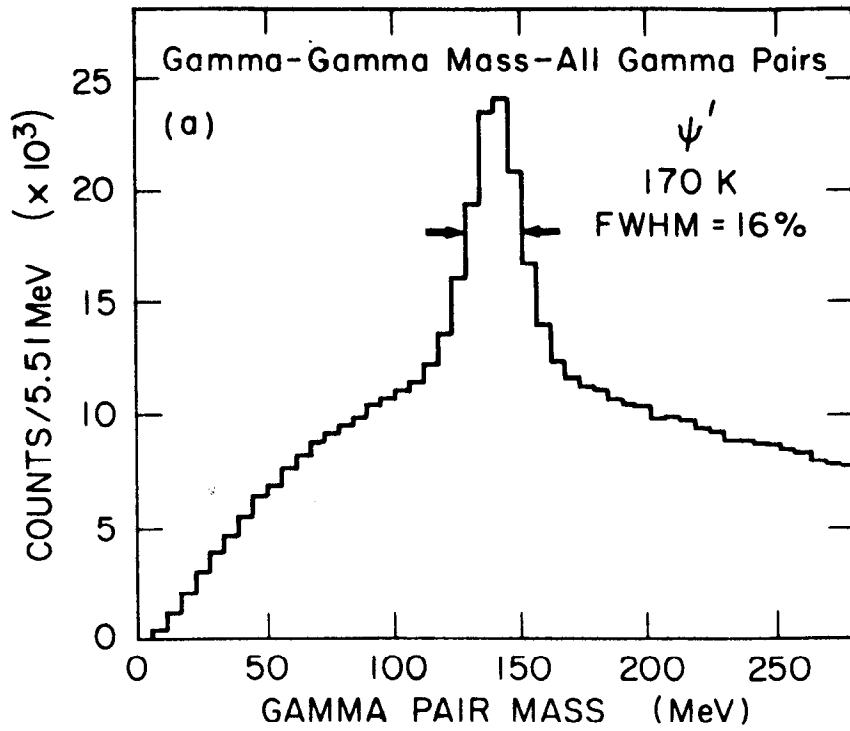
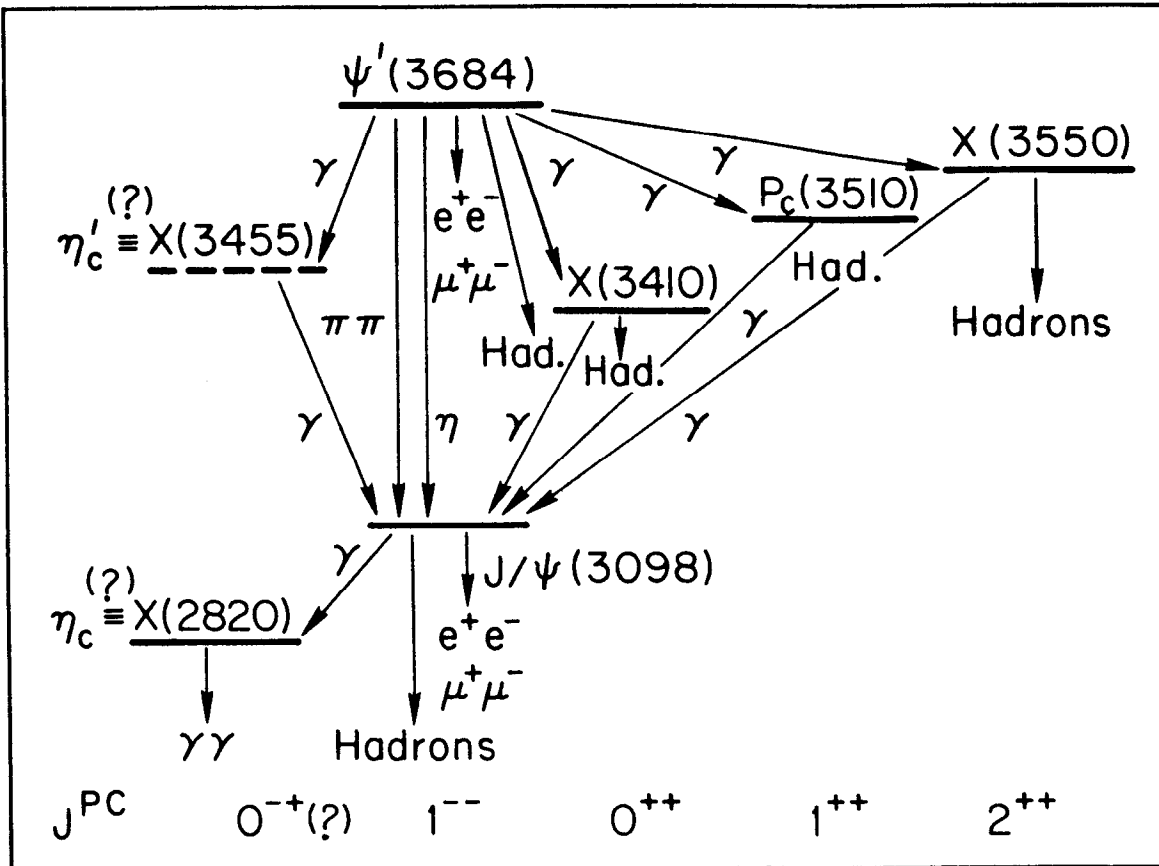
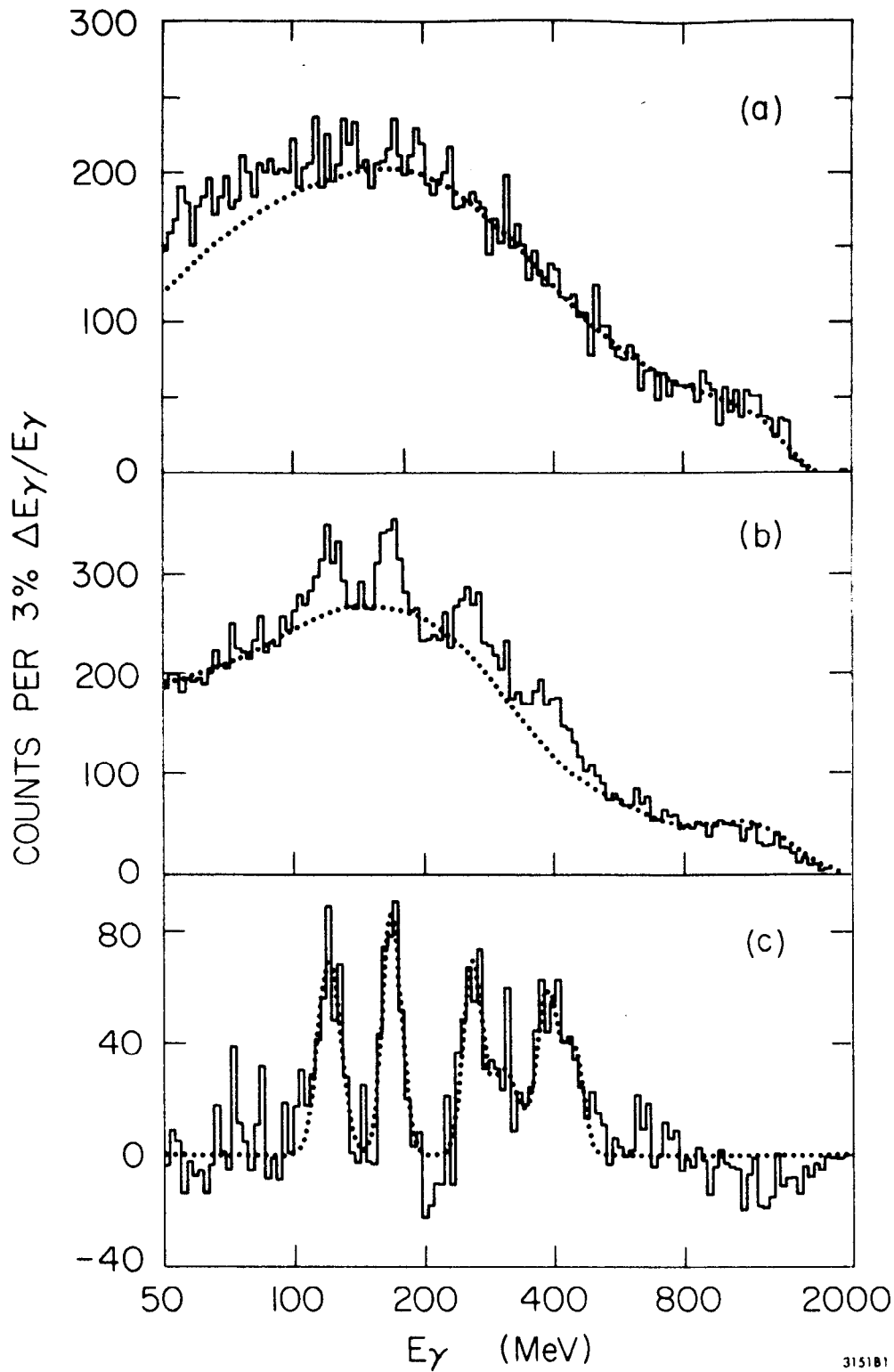


Fig. 10  
a)  $M_{\gamma\gamma}$  at  $\psi'$ , in region of  $\pi^0$   
b)  $M_{\gamma\gamma}$  at  $\psi$ , in region of  $\eta$



EXPERIMENTAL KNOWLEDGE  
OF THE CHARMONIUM STATES (1977)

Fig. 11



315181

Fig. 12  
 Inclusive  $\gamma$  spectra at  $\psi, \psi'$  from  
 $M P^2 S^3 D$

$\psi'$  INCLUSIVE  $\gamma$  SPECTRUM - EQUATOR, TUNNEL CUT

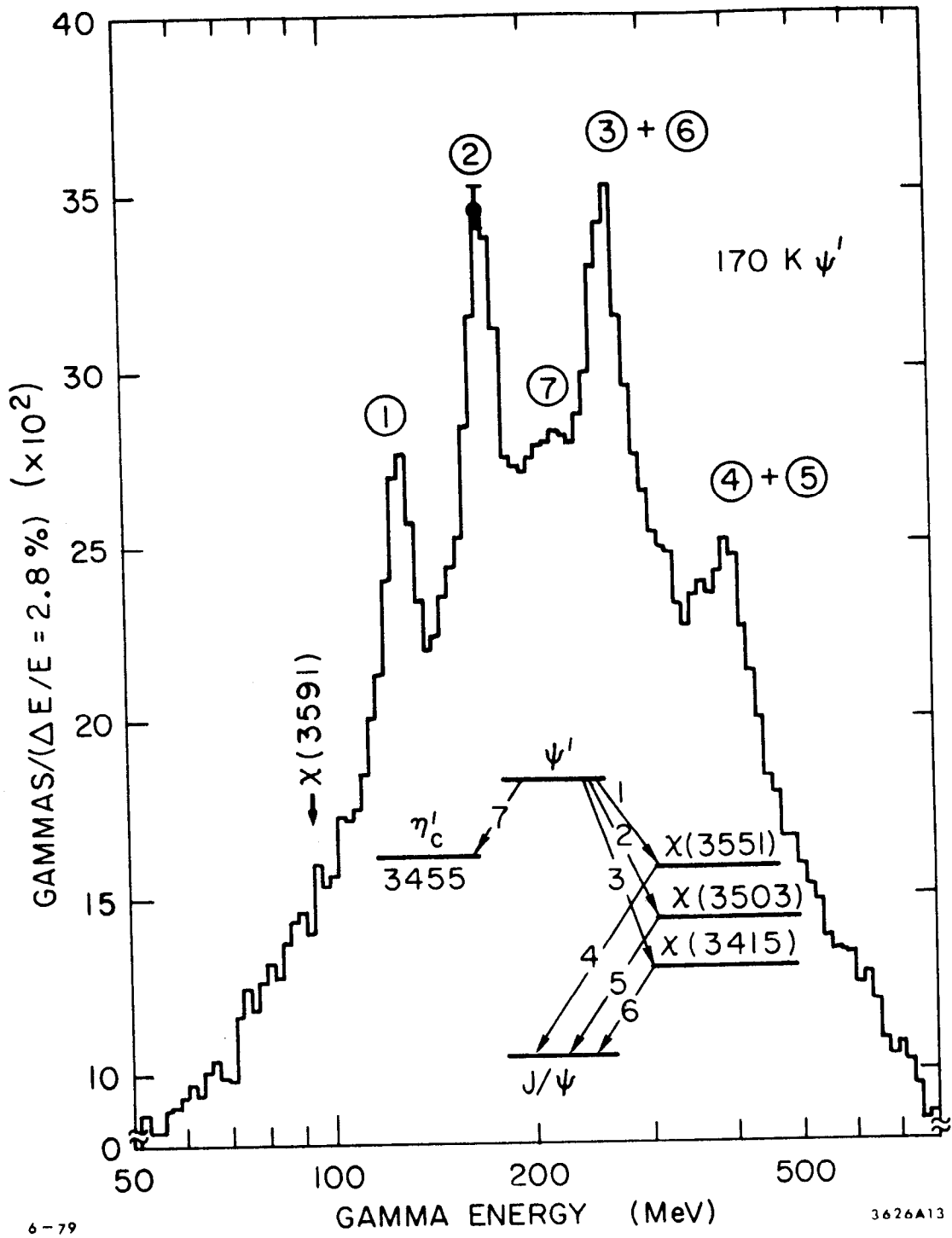


Fig. 13

Preliminary Crystal Ball inclusive  $\gamma$  spectrum at  $\psi'$

# $\psi'$ INCLUSIVE SPECTRUM

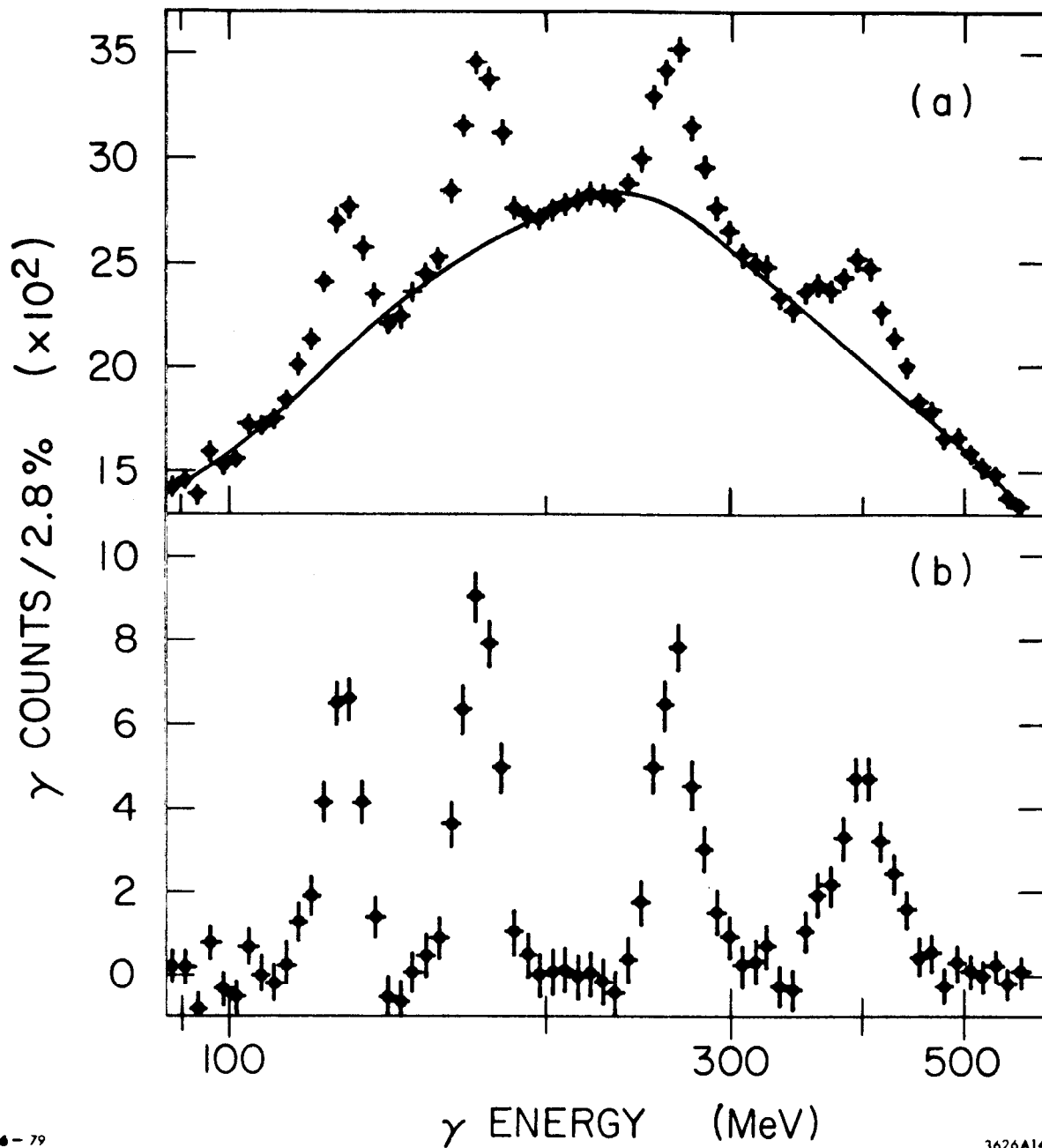
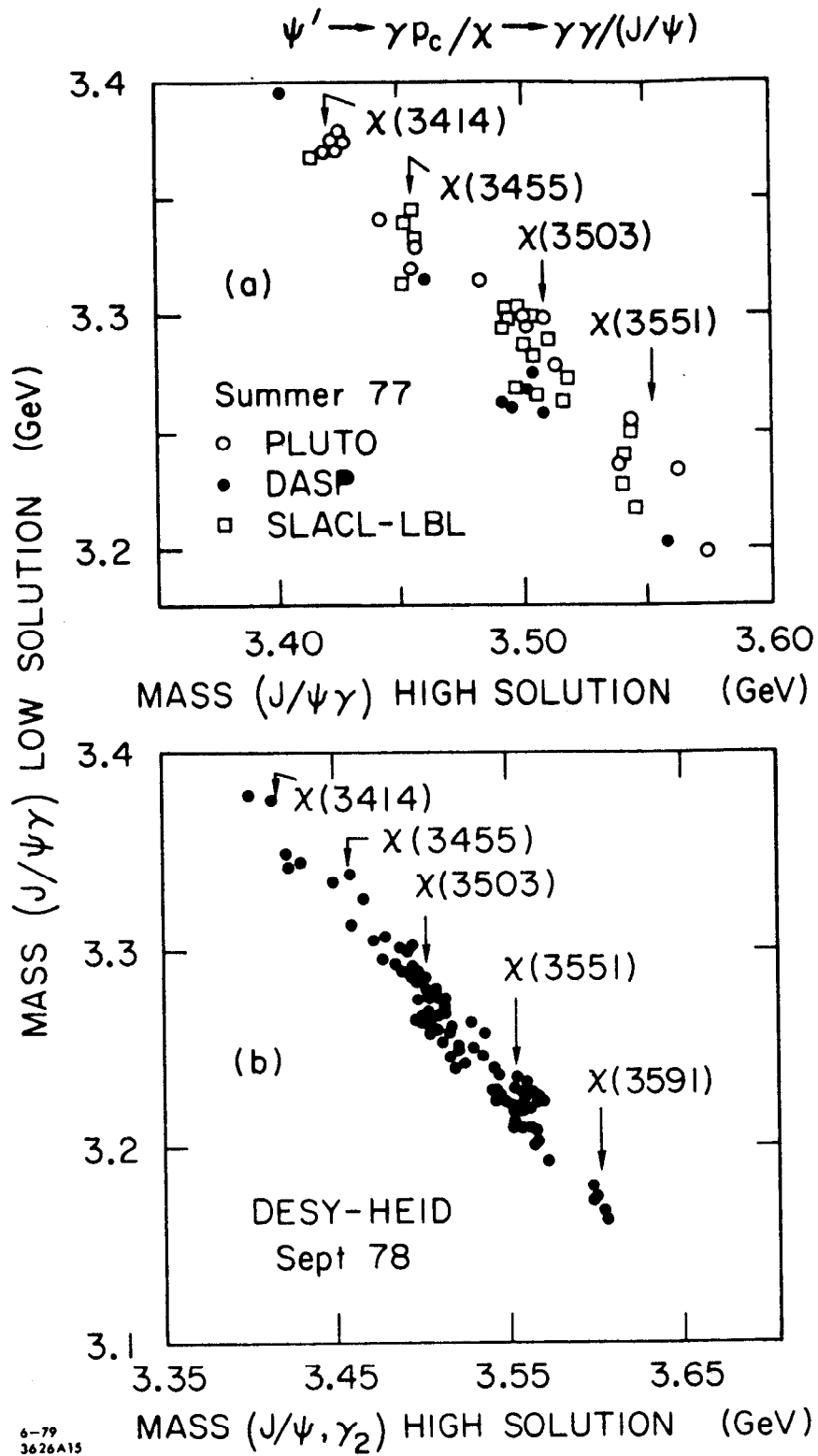


Fig. 14  
Inclusive  $\gamma$  spectrum a) with empirical background fit, b) fit subtracted.



6-79  
3626A15

Fig. 15  
 $E_{hi}^Y$  vs.  $E_{low}^Y$  plots for  $\psi' \rightarrow \gamma$   
 cascades: a) state of knowledge 1977  
 b) DESY-Heidelberg

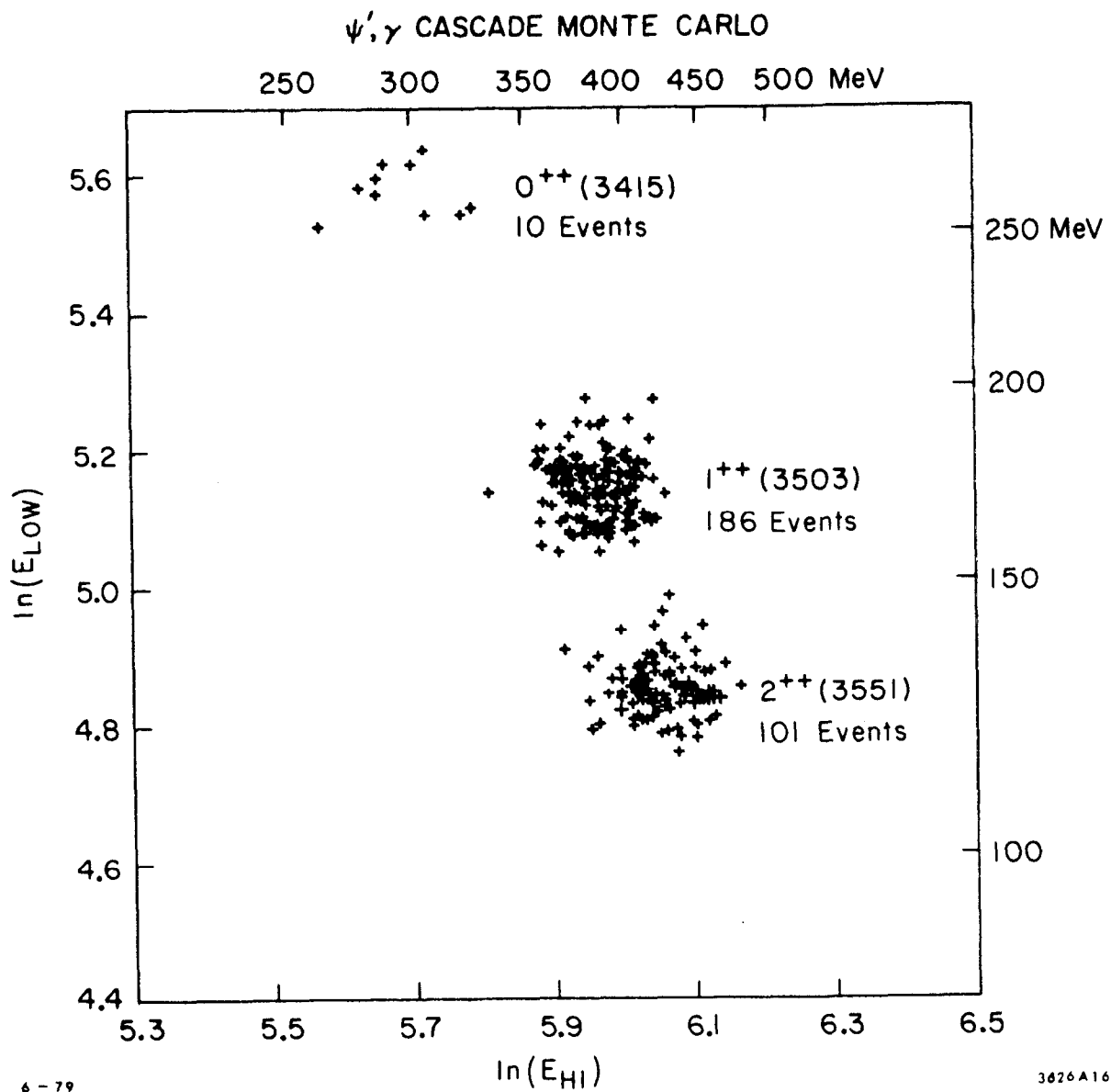


Fig. 16  
 Monte Carlo simulation for Crystal  
 Ball,  $\psi' \rightarrow \gamma$  Cascade

$\psi'$ ,  $\gamma$  CASCADE PRELIMINARY CRYSTAL BALL DATA

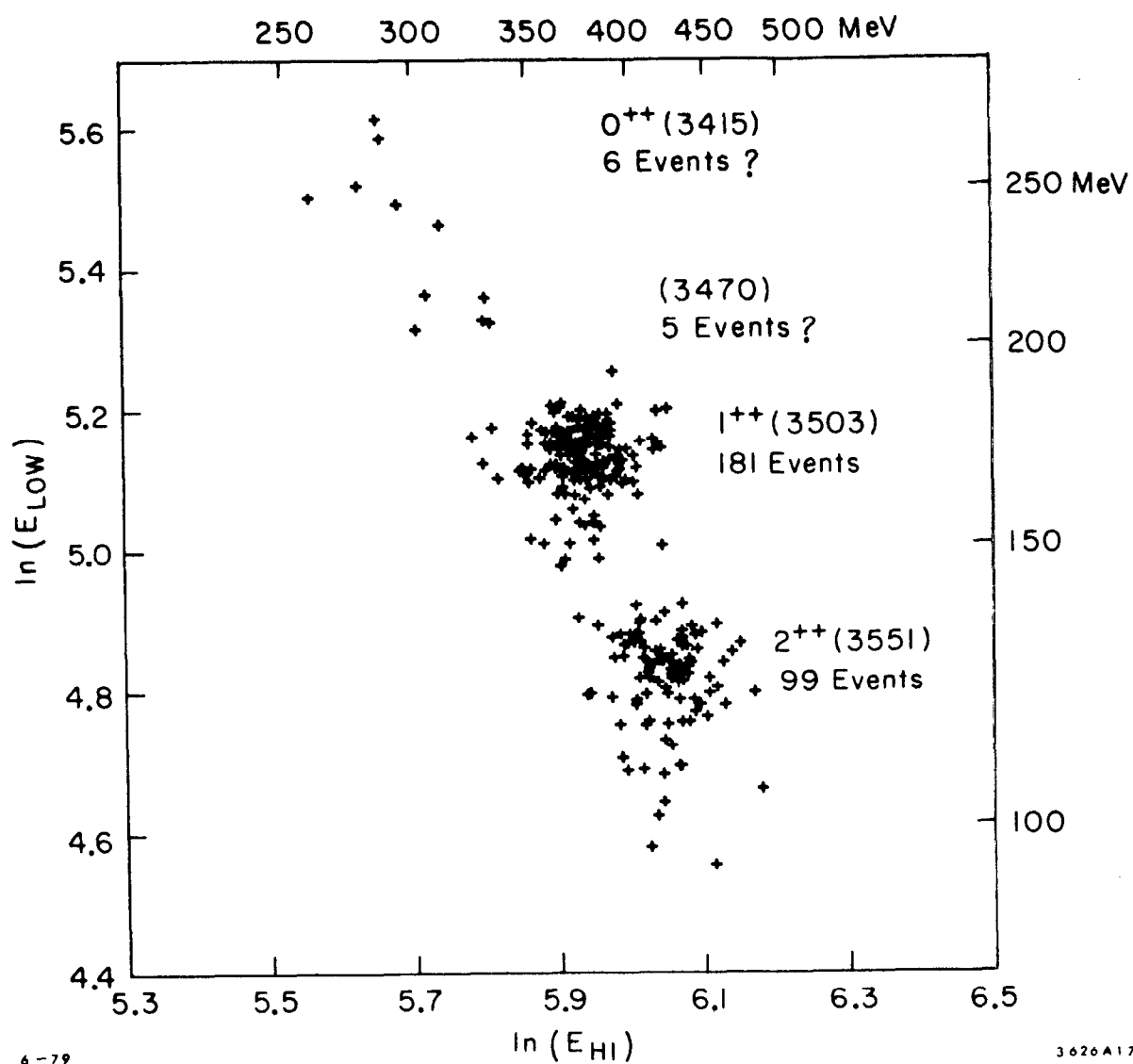


Fig. 17

$\pi^0$  SUBTRACTED

J/ $\psi$  INCLUSIVE GAMMA SPECTRUM

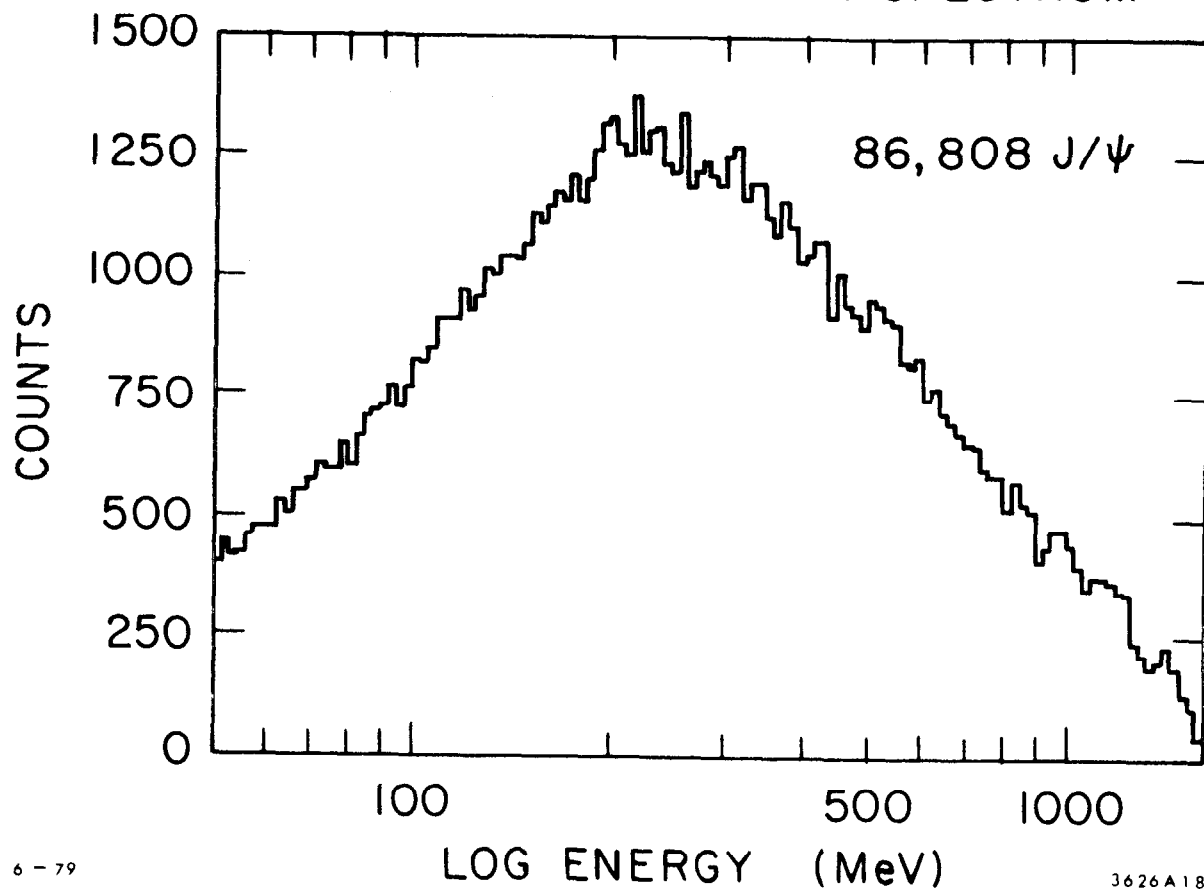


Fig. 18

Preliminary Crystal Ball inclusive  
 $\gamma$  spectrum at  $\psi$



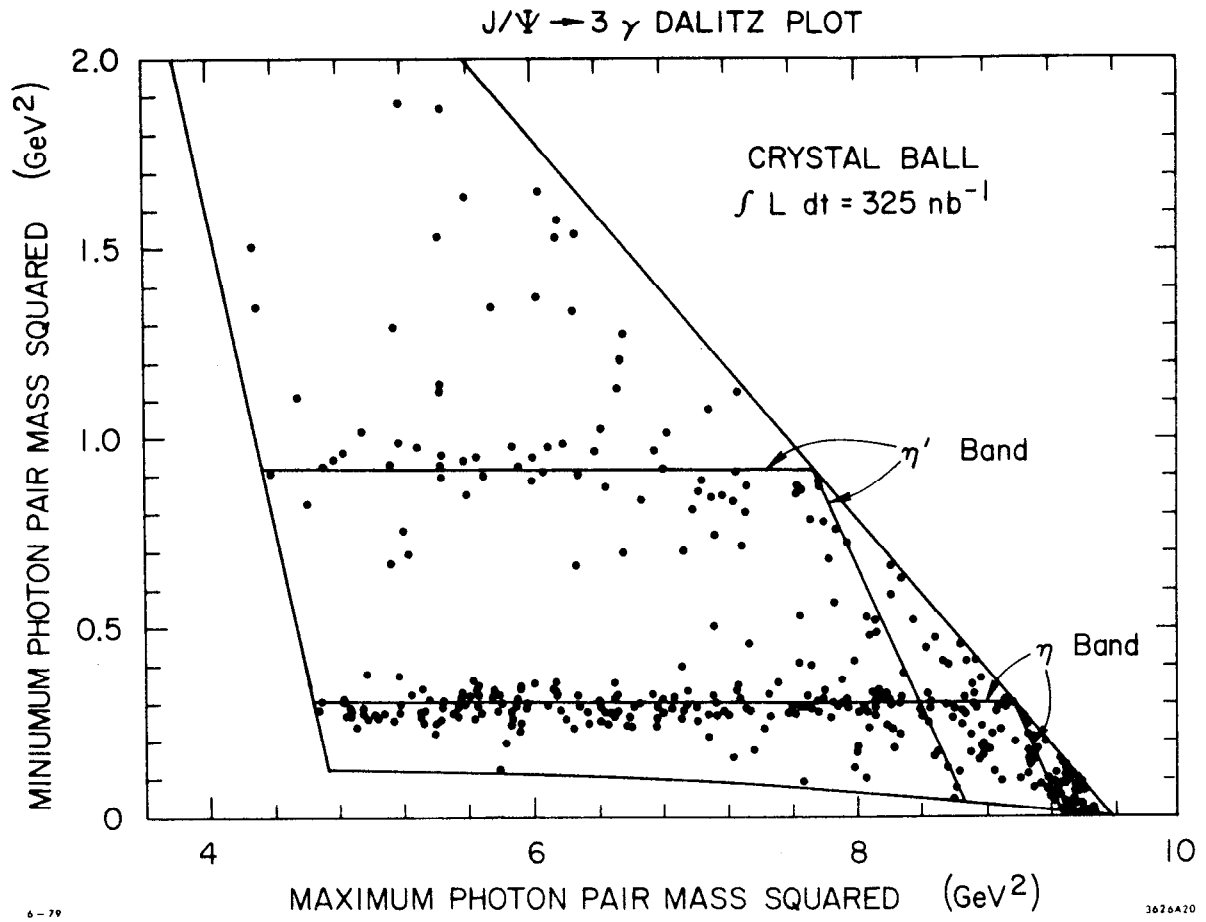


Fig. 20

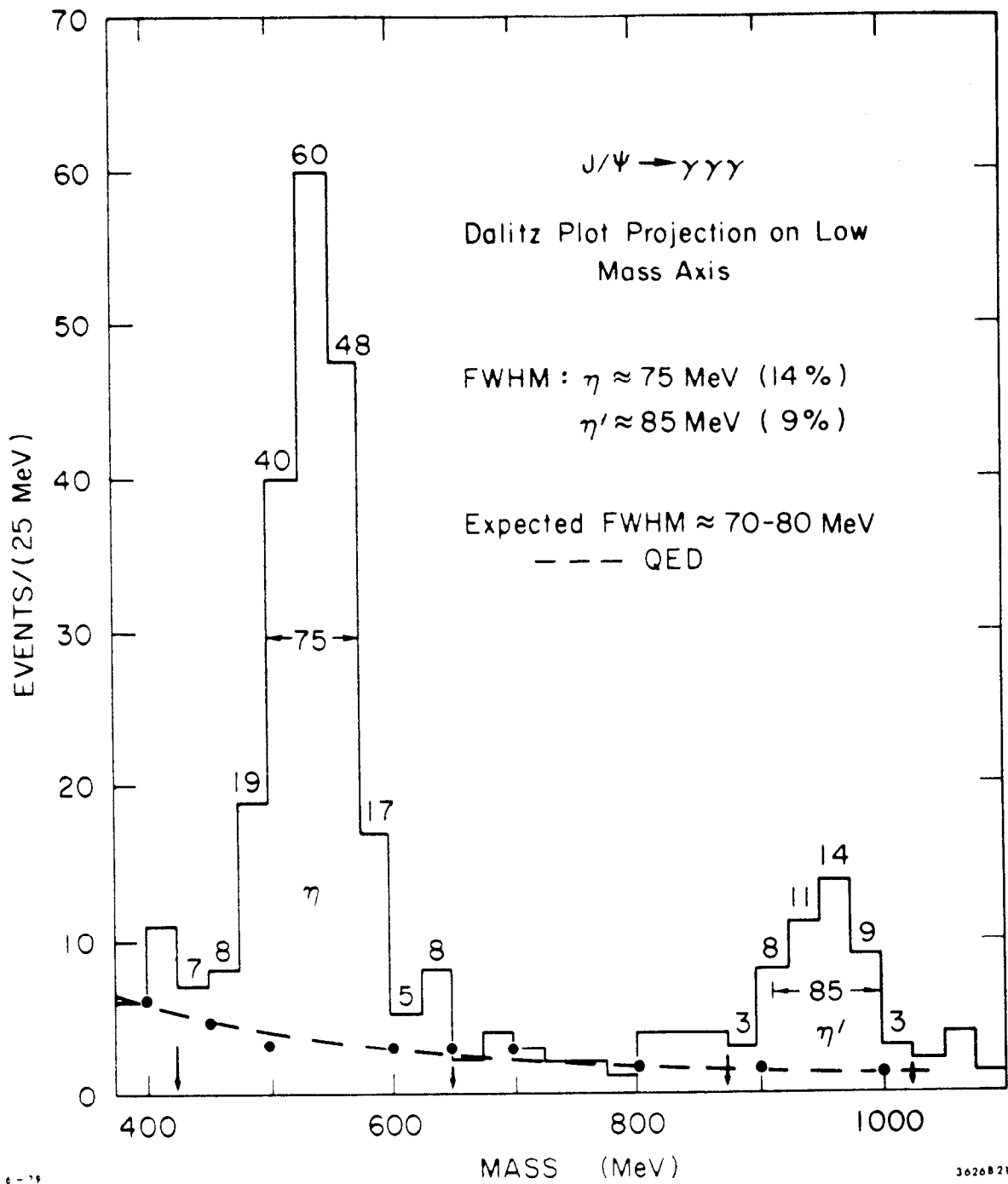


Fig. 21  
 Low mass projection of  $3\gamma$   
 Dalitz Plot

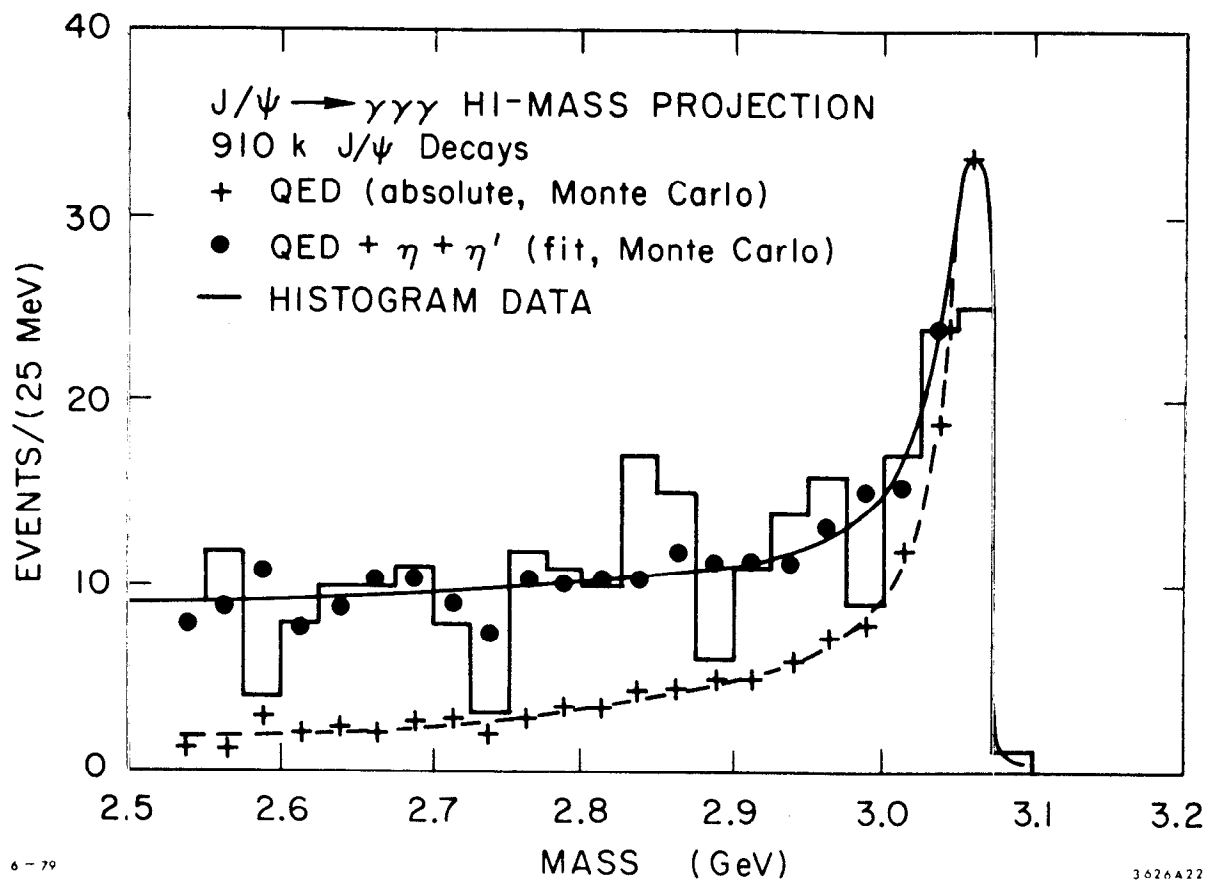


Fig. 22  
 High mass projection of  $3\gamma$   
 Dalitz plot